

Coulomb renormalization and ratio of proton and neutron asymptotic normalization coefficients for mirror nuclei

A. M. Mukhamedzhanov

Cyclotron Institute, Texas A&M University, College Station, Texas 77843, USA

(Received 9 September 2012; published 15 October 2012)

Asymptotic normalization coefficients (ANCs) are fundamental nuclear constants playing an important role in nuclear reactions, nuclear structure, and nuclear astrophysics. In this paper the physical reasons for the Coulomb renormalization of the ANC are addressed. Using the Pinkston-Satchler equation the ratio for the proton and neutron ANCs of mirror nuclei is obtained in terms of the Wronskians from the radial overlap functions and regular solutions of the two-body Schrödinger equation with the short-range interaction excluded. This ratio allows one to use microscopic overlap functions for mirror nuclei in the internal region, where they are the most accurate, to correctly predict the ratio of the ANCs for mirror nuclei, which determine the amplitudes of the tails of the overlap functions. Calculations presented for different nuclei demonstrate the Coulomb renormalization effects and independence of the ratio of the nucleon ANCs for mirror nuclei on the channel radius. This ratio is valid both for bound states and resonances. One of the goals of this paper is to draw attention to the possibility of using the Coulomb renormalized ANCs rather than the standard ones, especially when the standard ANCs are too large.

DOI: [10.1103/PhysRevC.86.044615](https://doi.org/10.1103/PhysRevC.86.044615)

PACS number(s): 21.10.Jx, 21.60.De, 03.65.Nk, 11.55.-m

I. INTRODUCTION

The asymptotic normalization coefficient (ANC) is a fundamental nuclear characteristic of bound states [1,2] and resonances (the partial resonance width is also expressed in terms of the ANC) [3,4] and plays an important role in nuclear reaction and structure physics. The ANCs determine the normalization of the peripheral part of transfer reaction amplitudes [1,2] and overall normalization of the peripheral radiative capture processes [5–8]. In the R -matrix approach the ANC determines the normalization of the external nonresonant radiative capture amplitude and the channel radiative reduced width amplitude [3,9,10].

The ANC enters the theory in two ways [1]. In the scattering theory the residue at the poles of the elastic scattering S matrix corresponding to bound states [11,12] or resonances [4] can be expressed in terms of the ANC,

$$S_{l_B j_B; l_B j_B}^{J_B} \xrightarrow{k \rightarrow k_{aA}^p} \frac{A_{l_B j_B}}{k - k_{aA}^p}, \quad (1)$$

with the residue

$$A_{l_B j_B}^{J_B} = -i^{2l_B+1} e^{i\pi\eta_{aA}^p} (C_{aA l_B j_B J_B}^B)^2, \quad (2)$$

where $C_{aA l_B j_B J_B}^B$ is the ANC for the virtual or real decay $B \rightarrow a + A$ in the channel with the relative orbital angular momentum l_B of a and A , the total angular momentum J_B of a , and total angular momentum J_B of the system $a + A$. If $B = (aA)$ is a bound state,

$$\eta_{aA}^p \equiv \eta_{aA}^{bs} = \frac{Z_a Z_A e^2 \mu_{aA}}{\kappa_{aA}^B} \quad (3)$$

is the Coulomb parameter for the bound state $B = (aA)$, $k_{aA}^p = i\kappa_{aA}^B$, $\kappa_{aA}^B = \sqrt{2\mu_{aA} \varepsilon_{aA}^B}$ is the bound-state wave number, $\varepsilon_{aA}^B = m_a + m_A - m_B$ is the binding energy for the virtual decay $B \rightarrow a + A$, $Z_i e$ and m_i is the charge and mass of

particle i , and μ_{aA} is the reduced mass of a and A . Throughout the paper I use the system of units in which $\hbar = c = 1$. Note that singling out the factor $e^{i\pi\eta_{aA}^p}$ in the residue makes the ANC for bound states real (see Sec. III B).

If B is a resonance, that is the decay $B \rightarrow a + A$ is real, then

$$\eta_{aA}^p = i\eta_{aA}^R, \quad \eta_{aA}^R = \frac{Z_a Z_A e^2 \mu_{aA}}{k_{aA}^R} \quad (4)$$

is the Coulomb parameter for the resonance state with complex relative momentum $k_{aA}^p = k_{aA}^R$, $k_{aA}^R = \sqrt{2\mu_{aA} E_{aA}^R}$, E_{aA}^R is the resonance energy in the system $a + A$ of the resonance state $B = (aA)$. Equations (1) and (2), being universally valid for both bound-state poles and resonances [4], provide the most general and model-independent definition of the ANC.

In the case of the Breit-Wigner resonance ($\text{Im } k_{aA}^R \ll \text{Re } k_{aA}^R = k_{aA}^0$) the residue of the elastic scattering S -matrix element in terms of the resonance width is

$$A_{l_B j_B}^{J_B} = -i e^{2i\delta_{l_B j_B}^p(k_{aA}^0)} \frac{\mu_{aA}}{k_{aA}^0} \Gamma_{aA l_B j_B J_B}, \quad (5)$$

where $\delta_{l_B j_B}^p(k_{aA}^0)$ is the potential (nonresonance) scattering phase shift at the real resonance relative momentum k_{aA}^0 . In the meantime, Eq. (2) in the Breit-Wigner resonance case takes the form

$$A_{l_B j_B}^{J_B} = -i^{2l_B+1} e^{-\pi\eta_{aA}^{(0)}} (C_{aA l_B j_B J_B}^B)^2, \quad (6)$$

where $\eta_{aA}^{(0)} = Z_a Z_A e^2 \mu_{aA} / k_{aA}^0$. Then the ANC and the partial width of the resonance are related by

$$(C_{aA l_B j_B J_B}^B)^2 = (-1)^{l_B} e^{\pi\eta_{aA}^{(0)}} e^{i2\delta_{l_B j_B}^p(k_{aA}^0)} \frac{\mu_{aA} \Gamma_{aA l_B j_B J_B}}{k_{aA}^0}. \quad (7)$$

In the case of the subthreshold resonance (the resonance which is a bound state in the entry channel and a resonance in the exit channel) the connection between the ANC and the partial width, calculated at the relative momentum of particles a and A k_{aA} , is given by [3]

$$\Gamma_{aAl_B j_B J_B}(k_{aA}) = P_{l_B}(k_{aA} R_{aA}) \frac{W_{-\eta_{aA}^{bs}, l_B+1/2}^2(2\kappa_{aA}^B R_{aA})}{\mu_{aA} R_{aA}} (C_{aAl_B j_B J_B}^B)^2, \quad (8)$$

where $P_{l_B}(k_{aA} R_{aA})$ is the barrier penetrability, $W_{-\eta_{aA}^{bs}, l_B+1/2}(2\kappa_{aA}^B R_{aA})$ is the Whittaker function for the bound state $B = (aA)$ and R_{aA} is the channel radius. Correspondingly, the reduced width is determined by

$$\gamma_{aAl_B j_B J_B}^2 = \frac{W_{-\eta_{aA}^{bs}, l_B+1/2}^2(2\kappa_{aA}^B R_{aA})}{2\mu_{aA} R_{aA}} (C_{aAl_B j_B J_B}^B)^2. \quad (9)$$

Note that in the R -matrix method the peripheral part of the radiative capture amplitude is expressed in terms of the reduced width rather than the ANC. However, the reduced width is model dependent, because it depends on the channel radius R_{aA} , while the ANC is not.

However, in the Schrödinger formalism of the wave functions the ANC is defined as the amplitude of the tail of the overlap function of the bound-state wave functions of B , A , and a . The overlap function is given by

$$\begin{aligned} I_{aA}^B(\mathbf{r}_{aA}) &= \langle \psi_c | \varphi_B(\xi_A, \xi_a; \mathbf{r}_{aA}) \rangle \\ &= \sum_{l_B m_{l_B} j_B m_{j_B}} \langle J_A M_A j_B m_{j_B} | J_B M_B \rangle \\ &\quad \times \langle J_a M_a l_B m_{l_B} | j_B m_{j_B} \rangle \\ &\quad \times Y_{l_B m_{l_B}}(\hat{\mathbf{r}}_{aA}) I_{aAl_B j_B J_B}^B(r_{aA}). \end{aligned} \quad (10)$$

Here

$$\begin{aligned} \psi_c &= \sum_{m_{j_B} m_{l_B} M_A M_a} \langle J_A M_A j_B m_{j_B} | J_B M_B \rangle \langle J_a M_a l_B m_{l_B} | j_B m_{j_B} \rangle \\ &\quad \times \hat{A}_{aA} \{ \varphi_A(\xi_A) \varphi_a(\xi_a) Y_{l_B m_{l_B}}(\hat{\mathbf{r}}_{aA}) \} \end{aligned} \quad (11)$$

is the two-body $a + A$ channel wave function in the $j j$ coupling scheme, $\langle j_1 m_1 j_2 m_2 | j m \rangle$ is the Clebsch-Gordan coefficient, \hat{A}_{aA} is the antisymmetrization operator between the nucleons of nuclei a and A , $\varphi_i(\xi_i)$ represents the fully antisymmetrized bound-state wave function of nucleus i with ξ_i being a set of the internal coordinates including spin-isospin variables, and J_i and M_i are the spin and spin projection, respectively, of nucleus i . Also, \mathbf{r}_{aA} is the radius vector connecting the centers of mass of nuclei a and A , $\hat{\mathbf{r}}_{aA} = \mathbf{r}_{aA}/r_{aA}$, $Y_{l_B m_{l_B}}(\hat{\mathbf{r}}_{aA})$ is the spherical harmonics, and $I_{aAl_B j_B J_B}^B(r_{aA})$ is the radial overlap function. The summation over l_B and j_B is carried out over the values allowed by the angular momentum and parity conservation in the virtual process $B \rightarrow A + a$.

The radial overlap function is given by

$$\begin{aligned} I_{aAl_B j_B J_B}^B(r_{aA}) &= \langle \hat{A}_{aA} \{ \varphi_A(\xi_A) \varphi_a(\xi_a) Y_{l_B m_{l_B}}(\hat{\mathbf{r}}_{aA}) \} | \varphi_B(\xi_A, \xi_a; \mathbf{r}_{aA}) \rangle \\ &= \left(\frac{A}{a} \right)^{\frac{1}{2}} \langle \varphi_A(\xi_A) \varphi_a(\xi_a) Y_{l_B m_{l_B}}(\hat{\mathbf{r}}_{aA}) | \varphi_B(\xi_A, \xi_a; \mathbf{r}_{aA}) \rangle. \end{aligned} \quad (12)$$

Equation (12) follows from a trivial observation that, because φ_B is fully antisymmetrized, the antisymmetrization operator \hat{A}_{aA} can be replaced by the factor

$$\left(\frac{A}{a} \right)^{\frac{1}{2}}.$$

In what follows, in contrast to Blokhintsev *et al.* [1], we absorb this factor into the radial overlap function.

The tail of the radial overlap function ($r_{aA} > R_{aA}$) in the case of the normal asymptotic behavior is given by

$$\begin{aligned} I_{aAl_B j_B J_B}^B(r_{aA}) &\xrightarrow{r_{aA} > R_{aA}} C_{aAl_B j_B J_B}^B \frac{W_{-\eta_{aA}^{bs}, l_B+1/2}(2\kappa_{aA}^B r_{aA})}{r_{aA}} \\ &\xrightarrow{r_{aA} \rightarrow \infty} C_{aAl_B j_B J_B}^B \frac{e^{-\kappa_{aA}^B r_{aA} - \eta_{aA}^{bs} \ln(2\kappa_{aA}^B r_{aA})}}{r_{aA}}. \end{aligned} \quad (13)$$

Correspondingly, for the resonance case,

$$\begin{aligned} I_{aAl_B j_B J_B}^B(r_{aA}) &\xrightarrow{r_{aA} > R_{aA}} C_{aAl_B j_B J_B}^B \frac{W_{-i\eta_{aA}^R, l_B+1/2}(-2i\kappa_{aA}(R)r_{aA})}{r_{aA}} \\ &\xrightarrow{r_{aA} \rightarrow \infty} C_{aAl_B j_B J_B}^B \frac{e^{i\kappa_{aA}(R)r_{aA} - i\eta_{aA}^R \ln(-2i\kappa_{aA}(R)r_{aA})}}{r_{aA}}. \end{aligned} \quad (14)$$

The proof of the fundamental connection between the residue $A_{l_B j_B}^{J_B}$ in the bound-state pole of the elastic scattering S matrix and the amplitude $C_{aAl_B j_B J_B}^B$ of the tail of the overlap function was presented for the first time in Ref. [11] and later on in Refs. [13–16]. The proof of this relationship for nonspherical potentials was given in Ref. [17] and for charged particles in Ref. [12]. Finally, generalization of this relationship for general case of bound state and resonances for charged particles was presented in Ref. [4].

The first comprehensive review about the overlap functions and ANC was given in Ref. [1], in which the theory of the ANC and its role in the nuclear reaction theory was presented. In another review paper [2], the role of the ANC in the theory of nuclear reactions with charged particles was addressed. The role of the ANC in nuclear astrophysics was discussed for the first time in Refs. [5,6], where it was underscored that the ANC determines the overall normalization of the peripheral radiative capture reactions. These two works cleared the way for using the ANC method as an indirect method in nuclear astrophysics (see also Ref. [18]). The ANC can be determined from peripheral transfer reactions and can be used to calculate peripheral radiative capture reactions. It constitutes a powerful indirect ANC method in nuclear astrophysics. The ANC method was extensively used in the analysis of

many important astrophysical reactions (see, for example, Refs. [8–10,19–24] and references therein). The role of the ANC in nuclear astrophysics has been once again underscored in the review [25].

Recently, it was shown that in the exact approach the only model-independent quantity, which can be determined from the analysis of nuclear reactions, is the ANC rather than the spectroscopic factor [26]. Moreover, in Ref. [27] a new formalism of the deuteron stripping based on the surface integral formalism and generalized R -matrix approach has been developed. It makes the role of the ANC in nuclear reactions theory even more important than it was thought to be before. In this formalism the amplitude of the deuteron stripping reactions populating bound states and resonances is parametrized in terms of the ANC rather than the spectroscopic factors.

In Ref. [28] the charge symmetry of strong interactions was used to relate the proton and neutron ANCs of the one-nucleon overlap integrals for light mirror nuclei. Equation (7) from Ref. [28], determining the ratio of the proton and neutron ANCs of mirror nuclei, allows us to find one of the ANCs if another one is known. This relation extends to the case of real proton decay where the mirror analog is a virtual neutron decay of a loosely bound state. In this case, a link is obtained between the proton width and the squared ANC of the mirror neutron state. The relation between mirror overlaps was used to study astrophysically relevant proton-capture reactions based on information obtained from transfer reactions with stable beams [29,30].

In Ref. [31] the impact of the particle continuum on the proton and neutron ANCs for mirror p - and d -shell nuclei within the framework of the real-energy and complex-energy continuum shell-model approaches. The authors consider the basic properties of the single-particle ANCs for charged and neutral particles as functions of the Coulomb parameter, binding energy and the orbital angular momentum. The authors investigate the validity of the ratio of the proton and neutron mirror ANCs given by Eq. (7) from Ref. [28]. The main finding of Ref. [31] is that the key factor affecting the ratio of the mirror ANCs is the distribution of the spectroscopic strength.

In Ref. [32] the model independence of the ratio of the proton and neutron ANCs for mirror nuclei was tested within a phenomenological model, where the valence nucleon moves in a deformed mean field of the core which is allowed to excite.

The calculations show that the ratio of the proton and neutron ANCs (see Table II from Ref. [28]) increases dramatically with decrease of the proton binding energy and the charge of the core. This is the result of the impact of the Coulomb barrier, which blocks the proton bound-state wave function in the nuclear interior, significantly decreasing its tail. Because the wave function is still normalized to unity, the drop of the radial tail is compensated by a corresponding increase of the amplitude of the tail. For loosely bound states and high charges the conventionally determined ANC becomes enormously huge, creating problems in computations. For example, the square of the proton ANC $^{21}\text{Na}(1/2^+, 2.425 \text{ MeV}) \rightarrow ^{20}\text{Ne} + p$ is $6.14 \times 10^{33} \text{ fm}^{-1}$ [21]. The square of the ANC for $^{17}\text{O}(6.356 \text{ MeV}, 1/2^+) \rightarrow ^{13}\text{C} + \alpha$ is $\sim 10^{168} \text{ fm}^{-1}$ [33]. In this paper I give a physical insight into factors determining

the Coulomb renormalization of the ANC, making it easier to compare the ANCs of mirror nuclei. The analysis of the Coulomb renormalization of the ANC is done using two approaches: the model-independent analytic structure of the scattering amplitude and the Pinkston-Satchler equation [34,35]. All the factors, which affect the ANC owing to the Coulomb interaction, are analyzed. As a result of this research I suggest using in the future analysis of the data on the renormalized proton ANC, in which the main Coulomb renormalization factor is excluded. It is especially useful in cases of high nuclei charges and low binding energies. I provide also a new expression for the ratio of the mirror ANCs based on the transformation of the expression for the overlap function obtained from the Pinkston-Satchler equation in terms of the Wronskian. This expression is especially useful when microscopic overlap functions are available. These microscopic overlap functions are usually accurate in the nuclear interior, which is enough to determine the ratio of the ANCs of the mirror nuclei expressed in terms of the Wronskian. Then if one of the ANCs is known experimentally, the second one can be determined.

II. COULOMB RENORMALIZATION OF THE ANC FROM ANALYTIC STRUCTURE OF THE SCATTERING AMPLITUDE

First, I address the Coulomb renormalization of the ANC from analytic structure of the scattering amplitude [2]. Let us consider the scattering of two charged spinless particles a and A (we disregard the spins because they do not affect the Coulomb renormalization). The analytic properties of the on-the-energy-shell Coulomb-nuclear partial wave scattering amplitude was investigated in Refs. [36–40]. The elastic scattering S -matrix element is given by

$$S_{l_B}(k_{aA}) = 1 + 2i \rho_{l_B}(k_{aA}) F_{l_B}(k_{aA}), \quad (15)$$

where $\rho_{l_B}(k_{aA}) = k_{aA}^{2l_B+1}$. The partial elastic scattering S -matrix element can be written as

$$S_{l_B}(k_{aA}) = e^{2i\delta_{l_B}} = S_{l_B}^C(k_{aA}) + S_{l_B}^C(k_{aA})[S_{l_B}^{\text{CN}}(k_{aA}) - 1], \quad (16)$$

$$S_{l_B}^C(k_{aA}) = e^{2i\delta_{l_B}^C} = \frac{\Gamma(l_B + 1 + i\eta_{aA})}{\Gamma(l_B + 1 - i\eta_{aA})} \quad (17)$$

which is the Coulomb elastic scattering S -matrix element and

$$S_{l_B}^{\text{CN}}(k_{aA}) = e^{2i\delta_{l_B}^{\text{CN}}} \quad (18)$$

is the Coulomb-modified nuclear elastic scattering S -matrix element, $\eta_{aA} = Z_1 Z_2 e^2 \mu_{aA}/k_{aA}$ is the Coulomb parameter of particles a and A in continuum, δ_{l_B} is the total scattering phase shift in the partial wave l_B , and $\delta_{l_B}^{\text{CN}} = \delta_{l_B} - \delta_{l_B}^C$ is the Coulomb-modified nuclear scattering phase shift. We rewrite the Coulomb-modified elastic scattering S -matrix element $S_{l_B}^{\text{CN}}(k_{aA})$ as

$$S_{l_B}^{\text{CN}}(k_{aA}) = e^{2i\delta_{l_B}^{\text{CN}}} = 1 + 2i \rho_{l_B}(k_{aA}) F_{l_B}^{\text{CN}}(k_{aA}). \quad (19)$$

The Coulomb-modified nuclear partial wave scattering amplitude $F_{l_B}^{\text{CN}}(k_{aA})$ is not an analytical function in the k_{aA}

plane [37]. Following Refs. [2,37] we can present

$$F_{l_B}^{\text{CN}}(k_{aA}) = \frac{1}{[h_{l_B}^C(k_{aA})]^2} T_{l_B}^{\text{CN}}(k_{aA}). \quad (20)$$

Here

$$h_{l_B}^C(k_{aA}) = \frac{l_B! e^{\frac{\pi}{2} \eta_{aA} \text{sgn}[\text{Re} k_{aA}]}{\Gamma(l_B + 1 + i \eta_{aA})} \quad (21)$$

is the normalized $[h_{l_B}^C(k_{aA}) \xrightarrow{k_{aA} \rightarrow \infty} 1]$ Coulomb Jost function. At real $k_{aA} > 0$ this definition coincides with a conventional definition of the Coulomb Jost function. Owing to the presence of the factor $\text{sign}[\text{Re} k_{aA}]$, $F_{l_B}^{\text{CN}}(k_{aA})$ has singularity along the imaginary axis in the k_{aA} plane, which splits $F_{l_B}^{\text{CN}}(k_{aA})$ into two parts corresponding to $\text{Re} k_{aA} > 0$ and $\text{Re} k_{aA} < 0$.

However, the singled-out renormalized Coulomb-modified nuclear partial wave scattering amplitude $T_{l_B}^{\text{CN}}(k_{aA})$ has the same analytical properties on the first (physical) sheet of the Riemann surface ($\text{Im} k_{aA} > 0$) as the pure nuclear partial wave scattering amplitude: right-hand unitarity cut ($0 \leq k_{aA} < \infty$) and left-hand ($E_{aA} < 0$) dynamical cut [2]. $T_{l_B}^{\text{CN}}(k_{aA})$, similar to the pure nuclear scattering amplitude, has a pole at $k_{aA} = i \kappa_{aA}^B$,

$$T_{l_B}^{\text{CN}}(k_{aA}) \xrightarrow{k_{aA} \rightarrow i \kappa_{aA}^B} \frac{\tilde{A}_{l_B}}{k_{aA} - i \kappa_{aA}^B}, \quad (22)$$

where the residue in the pole

$$\tilde{A}_{l_B} = -i^{2l_B+1} (\tilde{C}_{aAl_B}^B)^2. \quad (23)$$

Correspondingly, the residue of $F_{l_B}^{\text{CN}}(k_{aA})$ is

$$A_{l_B} = -i^{2l_B+1} e^{i\pi \eta_{aA}^{bs}} \left[\frac{\Gamma(l_B + 1 + \eta_{aA}^{bs})}{l_B!} \right]^2 (\tilde{C}_{aAl_B}^B)^2. \quad (24)$$

Here $\tilde{C}_{aAl_B}^B$ is the renormalized ANC, which is connected, according to Eq. (21), to the standard ANC [2]:

$$C_{aAl_B}^B = \frac{\Gamma(l_B + 1 + \eta_{aA}^{bs})}{l_B!} \tilde{C}_{aAl_B}^B. \quad (25)$$

As we can see, the standard ANC contains the Coulomb barrier factor $\frac{\Gamma(l_B+1+\eta_{aA}^{bs})}{l_B!}$. Correspondingly,

$$(C_{aAl_B}^B)^2 = \mathcal{R}_1 (\tilde{C}_{aAl_B}^B)^2. \quad (26)$$

where the renormalization factor in Eq. (26) is

$$\mathcal{R}_1 = \left[\frac{\Gamma(l_B + 1 + \eta_{aA}^{bs})}{l_B!} \right]^2, \quad (27)$$

TABLE I. The squared proton ANCs $(C_{pAl_B j_B J_B}^B)^2$ and Coulomb renormalized ANCs $(\tilde{C}_{pAl_B j_B J_B}^B)^2$ of the overlap functions $I_{pAl_B j_B J_B}^B$; $(l_B j_B J_B)$ are the quantum numbers of the removed proton and the total spin of nucleus B ; ε_{pA}^B is the binding energy for the virtual decay $B \rightarrow p + A$.

B	A	$l_B j_B$	J_B	ε_{pA}^B (MeV)	$(C_{pAl_B j_B}^B)^2 \text{ fm}^{-1}$	$(\tilde{C}_{pAl_B j_B}^B)^2 \text{ fm}^{-1}$
²¹ Na	²⁰ Ne(0.0 MeV)	$s_{1/2}$	1/2	0.0071	6.5×10^{33} [21]	2.66
⁵⁷ Cu	⁵⁶ Ni(0.0 MeV)	$p_{3/2}$	3/2	0.7	1.77×10^8 [41]	135
¹³² Sn	¹³¹ In(0.0 MeV)	$g_{9/2}$	0	15.71	9.03×10^8 [41]	1.22×10^6

which is derived only from consideration of the analytic properties of the elastic scattering amplitude. This factor is the main Coulomb renormalization factor (CRF) of the conventional ANC owing to the Coulomb barrier. It increases with increasing of charges and decreasing of the binding energy and can be quite huge.

Now we can rewrite the reduced width as (recovering the spins)

$$\gamma_{aAl_B j_B J_B}^2 = \frac{\tilde{W}_{-\eta_{aA}^{bs}, l_B+1/2}^2 (2\kappa_{aA}^B R_{aA})}{2\mu_{aA} R_{aA}} (\tilde{C}_{aAl_B j_B J_B}^B)^2, \quad (28)$$

where

$$\begin{aligned} \tilde{W}_{-\eta_{aA}^{bs}, l_B+1/2}^2 (2\kappa_{aA}^B R_{aA}) \\ = \frac{\Gamma(l_B + 1 + \eta_{aA}^{bs})}{l_B!} W_{-\eta_{aA}^{bs}, l_B+1/2}^2 (2\kappa_{aA}^B R_{aA}). \end{aligned} \quad (29)$$

The reduced width is given by the product of two factors. When the charge of nucleus increases and binding energy ε_{aA}^B decreases, the Coulomb barrier also increases, decreasing significantly the tail of the Whittaker function. However, owing to the conservation of the normalization of the bound-state wave function of nucleus B , the amplitude of the tail of the overlap function (its ANC) also significantly increases. Renormalization of the ANC and the Whittaker function, as is done in Eq. (29), decreases the ANC and increases the tail of the Whittaker function. This renormalization does not change the reduced width but allows one to operate with smaller ANCs than the standard ones and I draw the attention of the experimentalists to the possibility of using the Coulomb renormalized ANCs rather than the standard ones when the latter become too big.

I demonstrate the renormalization of the ANC in Table I.

III. ANC FROM PINKSTON-SATCHLER EQUATION

A. Coulomb renormalization of ANC from source term expression

Here we obtain the main CRF of the ANC using the equation for the ANC containing the source term [6,42]. To make it more clear, first we consider the derivation of this expression following Refs. [6,42] from the Pinkston-Satchler equation [34,35]. Note that the overlap function is not an eigenfunction of any Hermitian Hamiltonian. To derive the equation for the overlap function containing the source term, we start from the Schrödinger equation for the bound state of the parent

nucleus A :

$$(-\varepsilon_B - \widehat{T}_A - \widehat{T}_a - \widehat{T}_{aA} - V_a - V_A - V_{aA})\varphi_B(\xi_A, \xi_a; \mathbf{r}_{aA}) = 0. \quad (30)$$

Here, \widehat{T}_i is the internal motion kinetic energy operator of nucleus i , \widehat{T}_{aA} is the kinetic energy operator of the relative motion of nuclei a and A , V_i is the internal potential of nucleus i , V_{aA} is the interaction potential between a and A , and ε_B is the total binding energy of nucleus B .

Multiplying the Schrödinger equation (30) from the left by

$$\begin{aligned} & \binom{A}{a}^{1/2} \sum_{m_{j_B} m_{l_B} M_A M_a} \langle J_A M_A j_B m_{j_B} | J_B M_B \rangle \langle J_a M_a l_B m_{l_B} \\ & \times | j_B m_{j_B} \rangle Y_{l_B m_{l_B}}^*(\widehat{\mathbf{r}}_{aA}) \varphi_A^*(\xi_A) \varphi_a^*(\xi_a) \end{aligned} \quad (31)$$

and taking into account Eq. (12) we get the equation for the radial overlap function with the source term [42]

$$\begin{aligned} & (-\varepsilon_{aA}^B - \widehat{T}_{r_{aA}} - V_{l_B}^{\text{centr}} - U_{aA}^C) I_{aAl_B j_B J_B}^B(r_{aA}) \\ & = Q_{l_B j_B J_a J_A J_B}(r_{aA}). \end{aligned} \quad (32)$$

Here, $\widehat{T}_{r_{aA}}$ is the radial relative kinetic energy operator of the particles a and A , $V_{l_B}^{\text{centr}}$ is the centrifugal barrier for the relative motion of a and A with the orbital momentum l_B ; $Q_{l_B j_B J_a J_A J_B}(r_{aA})$ is the source term,

$$\begin{aligned} & Q_{l_B j_B J_a J_A J_B}(r_{aA}) \\ & = \sum_{m_{j_B} m_{l_B} M_A M_a} \langle J_A M_A j_B m_{j_B} | J_B M_B \rangle \langle J_a M_a l_B m_{l_B} | j_B m_{j_B} \rangle \\ & \times \binom{A}{a}^{1/2} \int d\Omega_{\mathbf{r}_{aA}} \langle \varphi_a(\xi_a) \varphi_A(\xi_A) | V_{aA} \\ & - U_{aA}^C | Y_{l_B m_{l_B}}^*(\widehat{\mathbf{r}}_{aA}) \varphi_B(\xi_a, \xi_A; \mathbf{r}_{aA}) \rangle. \end{aligned} \quad (33)$$

The integration in the matrix element $\langle \varphi_a(\xi_a) \varphi_A(\xi_A) | V_{aA} - U_{aA}^C | Y_{l_B m_{l_B}}^*(\widehat{\mathbf{r}}_{aA}) \varphi_B(\xi_a, \xi_A; \mathbf{r}_{aA}) \rangle$ in Eq. (33) is carried out over all the internal coordinates of nuclei a and A . Note that we replaced the antisymmetrization operator \widehat{A}_{aA} in Eq. (31) with

$$\binom{A}{a}^{1/2}$$

because the operator $E_B - \widehat{T}_A - \widehat{T}_a - \widehat{T}_{aA} - V_a - V_A - V_{aA}$ in Eq. (30) is symmetric over interchange of nucleons of a and A , while φ_B is antisymmetric. For charged particles it is convenient to single out the channel Coulomb interaction $U_{aA}^C(r_{aA})$ between the center of mass of nuclei a and A .

Equation (33) can be rewritten in the integral form:

$$\begin{aligned} I_{aAl_B j_B J_B}^B(r_{aA}) & = \frac{1}{r_{aA}} \int_0^\infty dr'_{aA} r'_{aA} G_{l_B}^C(r_{aA}, r'_{aA}; -\varepsilon_{aA}^B) \\ & \times Q_{l_B j_B J_a J_A J_B}(r'_{aA}). \end{aligned} \quad (34)$$

The partial Coulomb two-body Green's function is given by [43]

$$\begin{aligned} & G_{l_B}^C(r_{aA}, r'_{aA}; -\varepsilon_{aA}^B) \\ & = -2\mu_{aA} \frac{\varphi_{l_B}^C(i\kappa_{aA}^B r_{aA<}) f_{l_B}^{C(+)}(i\kappa_{aA}^B r_{aA>})}{L_{l_B}^{C(+)}(i\kappa_{aA}^B)}, \end{aligned} \quad (35)$$

where $r_{aA<} = \min\{r_{aA}, r'_{aA}\}$ and $r_{aA>} = \max\{r_{aA}, r'_{aA}\}$. The Coulomb regular solution $\varphi_{l_B}^C(i\kappa_{aA}^B r_{aA})$ of the partial Schrödinger equation at imaginary momentum $i\kappa_{aA}^B$ is

$$\begin{aligned} & \varphi_{l_B}^C(i\kappa_{aA}^B r_{aA}) \\ & = -\frac{1}{2\kappa_{aA}^B} [L_{l_B}^{C(-)}(i\kappa_{aA}^B) f_{l_B}^{C(+)}(i\kappa_{aA}^B, r_{aA}) \\ & - L_{l_B}^{C(+)}(i\kappa_{aA}^B) f_{l_B}^{C(-)}(i\kappa_{aA}^B, r_{aA})] \\ & = r_{aA}^{l_B+1} e^{-\kappa_{aA}^B r_{aA}} {}_1F_1(l_B+1+\eta_{aA}^{bs}, 2l_B+2; 2\kappa_{aA}^B r_{aA}) \\ & = e^{-i\pi l_B/2} L_{l_B}^{C(+)}(i\kappa_{aA}^B) \frac{e^{i\sigma_B} F_{l_B}(i\kappa_{aA}^B, r_{aA})}{i\kappa_{aA}^B}, \end{aligned} \quad (36)$$

where

$$\begin{aligned} & e^{i\sigma_B} F_{l_B}(i\kappa_{aA}^B, r_{aA}) \\ & = e^{i\pi \eta_{aA}^{bs}/2} \frac{\Gamma(l_B+1+\eta_{aA}^{bs})}{2\Gamma(2l_B+2)} (2i\kappa_{aA}^B r_{aA})^{l_B+1} e^{-\kappa_{aA}^B r_{aA}} \\ & \times {}_1F_1(l_B+1+\eta_{aA}^{bs}, 2l_B+2; 2\kappa_{aA}^B r_{aA}). \end{aligned} \quad (37)$$

Also,

$$f_{l_B}^{C(\pm)}(i\kappa_{aA}^B, r_{aA}) = e^{-i\pi \eta_{aA}^{bs}/2} W_{\mp \eta_{aA}^{bs}, l_B+1/2}(\pm 2\kappa_{aA}^B r_{aA}) \quad (38)$$

are the Jost solutions (singular at the origin $r_{aA} = 0$), and

$$\begin{aligned} L_{l_B}^{C(\pm)}(i\kappa_{aA}^B) & = \frac{1}{(2i\kappa_{aA}^B)^{l_B}} e^{-i\pi \eta_{aA}^{bs}/2} e^{\pm i\pi l_B/2} \\ & \times \frac{\Gamma(2l_B+2)}{\Gamma(l_B+1 \pm \eta_{aA}^{bs})} \end{aligned} \quad (39)$$

are the Jost functions.

The asymptotic behavior of the overlap function is correct because it is governed by the Green's function:

$$\begin{aligned} & I_{aAl_B j_B J_B}^B(r_{aA}) \\ & \underset{r_{aA} \rightarrow \infty}{\approx} -2\mu_{aA} \frac{W_{-\eta_{aA}^B, l_B+1/2}(2\kappa_{aA}^{bs} r_{aA})}{r_{aA}} \frac{e^{-i\pi \eta_{aA}^{bs}/2}}{L_{l_B}^{C(+)}(i\kappa_{aA}^B)} \\ & \times \int_0^{r_{aA}} dr'_{aA} r'_{aA} \varphi_{l_B}^C(i\kappa_{aA}^B r'_{aA}) Q_{l_B j_B J_a J_A J_B}(r'_{aA}). \end{aligned} \quad (40)$$

Taking into account Eq. (13) we get the ANC expressed in terms of the source $Q_{l_B j_B J_a J_A J_B}(r_{aA})$ [6,42]:

$$\begin{aligned} C_{aAl_B j_B J_B}^B & = -2\mu_{aA} e^{-i\pi \eta_{aA}^{bs}/2} \frac{1}{L_{l_B}^{C(+)}(i\kappa_{aA}^B)} \\ & \times \int_0^\infty dr_{aA} r_{aA} \varphi_{l_B}^C(i\kappa_{aA}^B r_{aA}) Q_{l_B j_B J_a J_A J_B}(r_{aA}). \end{aligned} \quad (41)$$

Owing to the presence of the short-range potential operator $V_{aA} - U_{aA}^C$ (potential V_{aA} is the sum of the nuclear V_{aA}^N and the Coulomb V_{aA}^C potentials and subtraction of U_{aA}^C removes the long-range Coulomb term from V_{aA}) the source term is

also a short-range function and we approximate Eq. (41) with

$$C_{aAl_B j_B J_B}^B \approx -2 \mu_{aA} e^{-i\pi \eta_{aA}^{bs}/2} \frac{1}{L_{l_B}^{C(+)}(i \kappa_{aA}^B)} \times \int_0^{R_{aA}} dr_{aA} r_{aA} \varphi_{l_B}^C(i \kappa_{aA}^B r_{aA}) \mathcal{Q}_{l_B j_B J_a J_A J_B}(r_{aA}), \quad (42)$$

where R_{aA} is the channel radius. This equation provides the ANC, which, as shown below, depends on R_{aA} and may not be accurate enough because we cut the integration over r_{aA} at the channel radius R_{aA} . However, here we are interested in the ratio of the mirror proton and neutron ANCs and, as demonstrated below, this ratio is practically insensitive to the value of the channel radius.

$[L_{l_B}^{C(+)}(i \kappa_{aA}^B)]^{-1}$ contains the same barrier $\Gamma(l_B + 1 + \eta_{aA}^{bs})$ [see Eq. (39)], which has been found in Sec. II based on the general principle of analyticity of the elastic scattering amplitude. Hence, following Eq. (25), we introduce the renormalized ANC

$$\tilde{C}_{aAl_B j_B J_B}^B \approx -2 \mu_{aA} (2 \kappa_{aA}^B)^{l_B} \frac{\Gamma(l_B + 1)}{\Gamma(2l_B + 2)} \times \int_0^{R_{aA}} dr_{aA} r_{aA} \varphi_{l_B}^C(i \kappa_{aA}^B r_{aA}) \mathcal{Q}_{l_B j_B J_a J_A J_B}(r_{aA}). \quad (43)$$

The conventional ANC is related to the renormalized one as

$$C_{aAl_B j_B J_B}^B = \frac{\Gamma(l_B + 1 + \eta_{aA}^{bs})}{l_B!} \tilde{C}_{aAl_B j_B J_B}^B. \quad (44)$$

B. ANC in terms of Wronskian

The advantage of Eq. (42) is that to calculate the ANC one needs to know the overlap function only in the nuclear interior where the *ab initio* methods such as no-core-shell-model [44–46], variational Green's function Monte Carlo method [47–49], and coupled-cluster method [50] are more accurate than in the external region. Now we transform the radial integral in Eq. (42) into the Wronskian at $r_{aA} = R_{aA}$. The philosophy of this transformation is the same as in the surface integral formalism [51–53] applied here only for bound states.

First we rewrite

$$V_{aA} - U_{aA}^C = V + V_{l_B}^{\text{centr}} - V_a - V_A - V_{l_B}^{\text{centr}} - U_{aA}^C \quad (45)$$

and take into account equations

$$\begin{aligned} (-\varepsilon_B - \hat{T}_a - \hat{T}_A - \hat{T}_{r_{aA}}) \varphi_{l_B}^C(i \kappa_{aA}^B r_{aA}) \varphi_a(\xi_a) \varphi_A(\xi_A) \\ = (U_{aA}^C + V_{l_B}^{\text{centr}} + V_a + V_A) \varphi_{l_B}^C(i \kappa_{aA}^B r_{aA}) \varphi_a(\xi_a) \varphi_A(\xi_A) \end{aligned} \quad (46)$$

and

$$(-\varepsilon_B - \hat{T}_a - \hat{T}_A - \hat{T}_{r_{aA}}) \langle Y_{l_B m_{l_B}}(\hat{\mathbf{r}}_{aA}) | \varphi_B \rangle = (V_{aA} + V_a + V_A + V_{l_B}^{\text{centr}}) \langle Y_{l_B m_{l_B}}(\hat{\mathbf{r}}_{aA}) | \varphi_B \rangle, \quad (47)$$

where $\hat{T}_{r_{aA}}$ is the radial kinetic energy operator. Then we get

$$\begin{aligned} C_{aAl_B j_B J_B}^B &\approx -2 \mu_{aA} e^{-i\pi \eta_{aA}^{bs}/2} \frac{1}{L_{l_B}^{C(+)}(i \kappa_{aA}^B)} \int_0^{R_{aA}} dr_{aA} r_{aA} \varphi_{l_B}^C(i \kappa_{aA}^B r_{aA}) \mathcal{Q}_{l_B j_B J_a J_A J_B}(r_{aA}) = -2 \mu_{aA} e^{-i\pi \eta_{aA}^{bs}/2} \\ &\times \frac{1}{L_{l_B}^{C(+)}(i \kappa_{aA}^B)} \sum_{m_j m_{l_B} M_A M_a} \langle J_A M_A j_B m_{j_B} | J_B M_B \rangle \langle J_a M_a l_B m_{l_B} | j_B m_{j_B} \rangle \binom{A}{a}^{1/2} \int_0^{R_{aA}} dr_{aA} r_{aA} \varphi_{l_B}^C(i \kappa_{aA}^B r_{aA}) \\ &\times \int d\Omega_{\mathbf{r}_{aA}} \langle \varphi_a(\xi_a) \varphi_A(\xi_A) | \overleftarrow{\hat{T}}_{r_{aA}} + \overleftarrow{\hat{T}}_a + \overleftarrow{\hat{T}}_A - \overrightarrow{\hat{T}}_a - \overrightarrow{\hat{T}}_A - \overrightarrow{\hat{T}}_{r_{aA}} | Y_{l_B m_{l_B}}^*(\hat{\mathbf{r}}_{aA}) \varphi_B(\xi_a, \xi_A; \mathbf{r}_{aA}) \rangle \\ &= -2 \mu_{aA} e^{-i\pi \eta_{aA}^{bs}/2} \frac{1}{L_{l_B}^{C(+)}(i \kappa_{aA}^B)} \sum_{m_j m_{l_B} M_A M_a} \langle J_A M_A j_B m_{j_B} | J_B M_B \rangle \langle J_a M_a l_B m_{l_B} | j_B m_{j_B} \rangle \\ &\times \binom{A}{a}^{1/2} \int_0^{R_{aA}} dr_{aA} r_{aA} \varphi_{l_B}^C(i \kappa_{aA}^B r_{aA}) \int d\Omega_{\mathbf{r}_{aA}} \langle \varphi_a(\xi_a) \varphi_A(\xi_A) | \overleftarrow{\hat{T}}_{r_{aA}} - \overrightarrow{\hat{T}}_{r_{aA}} | Y_{l_B m_{l_B}}^*(\hat{\mathbf{r}}_{aA}) \varphi_B(\xi_a, \xi_A; \mathbf{r}_{aA}) \rangle \\ &= -2 \mu_{aA} e^{-i\pi \eta_{aA}^{bs}/2} \frac{1}{L_{l_B}^{C(+)}(i \kappa_{aA}^B)} \int_0^{R_{aA}} dr_{aA} r_{aA} \varphi_{l_B}^C(i \kappa_{aA}^B r_{aA}) (\overleftarrow{\hat{T}}_{r_{aA}} - \overrightarrow{\hat{T}}_{r_{aA}}) I_{aAl_B j_B J_B}^B(r_{aA}). \end{aligned} \quad (48)$$

Taking into account that

$$\begin{aligned} f(x) \left(\frac{\overleftarrow{d}^2}{dx^2} - \frac{\overrightarrow{d}^2}{dx^2} \right) g(x) \\ = \frac{d}{dx} \left[g(x) \frac{df(x)}{dx} - f(x) \frac{dg(x)}{dx} \right], \end{aligned} \quad (49)$$

we arrive at the final expression for the ANC in terms of the Wronskian,

$$\begin{aligned} C_{aAl_B j_B J_B}^B &= e^{-i\pi \eta_{aA}^{bs}/2} \frac{1}{L_{l_B}^{C(+)}(i \kappa_{aA}^B)} \\ &\times W \left[I_{aAl_B j_B J_B}^B(r_{aA}), \varphi_{l_B}^C(i \kappa_{aA}^B r_{aA}) \right] \Big|_{r_{aA}=R_{aA}}, \end{aligned} \quad (50)$$

where the Wronskian

$$\begin{aligned} W_a(i\kappa_{aA}^B r_{aA}) &= W[I_{aAl_B j_B J_B}^B(r_{aA}), \varphi_{l_B}^C(i\kappa_{aA}^B r_{aA})] \\ &= I_{aAl_B j_B J_B}^B(r_{aA}) \frac{d\varphi_{l_B}^C(i\kappa_{aA}^B r_{aA})}{dr_{aA}} \\ &\quad - \varphi_{l_B}^C(i\kappa_{aA}^B r_{aA}) \frac{dI_{aAl_B j_B J_B}^B(r_{aA})}{dr_{aA}}. \end{aligned} \quad (51)$$

It is straightforward to see that determined here ANC is a real quantity because $\varphi_{l_B}^C(i\kappa_{aA}^B r_{aA})$ given by Eq. (36), $I_{aAl_B j_B J_B}^B(r_{aA})$, and $e^{-i\pi\eta_{aA}^{bs}/2} \frac{1}{L_{l_B}^{C(+)}(i\kappa_{aA}^B)}$ are real at pure imaginary momentum $k_{aA} = i\kappa_{aA}^B$. Correspondingly, the Coulomb renormalized ANC is given by

$$\begin{aligned} \tilde{C}_{aAl_B j_B J_B}^B &= (2\kappa_{aA}^B)^{l_B} \frac{\Gamma(l_B + 1)}{\Gamma(2l_B + 2)} \\ &\quad \times W[I_{aAl_B j_B J_B}^B(r_{aA}), \varphi_{l_B}^C(i\kappa_{aA}^B r_{aA})] \Big|_{r_{aA}=R_{aA}}. \end{aligned} \quad (52)$$

We know that the Wronskian calculated for two independent solutions of the Schrödinger equation is constant [43]. Because the radial overlap function $I_{aAl_B j_B J_B}^B(r_{aA})$ is not a solution of the Schrödinger equation in the nuclear interior, the Wronskian and, hence, the ANC determined by Eq. (48) depend on the channel radius R_{aA} , if it is not too large. However, if the adopted channel radius is large enough, we can replace the radial overlap function with its asymptotic term [see Eq. (13)] proportional to the Whittaker function, which determines the radial shape of the asymptotic radial overlap function and is a singular solution of the radial Schrödinger equation. Thus, because $\varphi_{l_B}^C(i\kappa_{aA}^B r_{aA})$ is an independent regular solution of the same equation, at large R_{aA} , where nuclear $a - A$ interaction can be neglected and asymptotic Eq. (13) can be applied, taking into account that $W[f_{l_B}^{C(+)}(i\kappa_{aA}^B, r_{aA}), f_{l_B}^{C(-)}(i\kappa_{aA}^B, r_{aA})] = 2\kappa_{aA}^B$ and Eq. (36) we get at large R_{aA}

$$\begin{aligned} e^{-i\pi\eta_{aA}^{bs}/2} \frac{1}{L_{l_B}^{C(+)}(i\kappa_{aA}^B)} W[I_{aAl_B j_B J_B}^B(r_{aA}), \\ \varphi_{l_B}^C(i\kappa_{aA}^B r_{aA})] \Big|_{r_{aA}=R_{aA}} &= C_{aAl_B j_B J_B}^B. \end{aligned} \quad (53)$$

Hence, Eq. (50) at large R_{aA} , as expected, turns into identity and proof of it is an additional test that Eq. (50) is correct. However, our idea is to use Eq. (48) at R_{aA} , which does not exceed the radius of nucleus $B = (aA)$. In the nuclear interior the contemporary microscopic models provide quite accurate

overlap functions. The ANC calculated using Eq. (48) may depend on the adopted channel radius R_{aA} but the ratio of the mirror ANCs, as shown below, practically is not sensitive to R_{aA} . It allows us to analyze the impact of the Coulomb effects on the ANC by separating different scales of these effects.

IV. COMPARISON OF MIRROR PROTON AND NEUTRON ANCS AND COULOMB EFFECTS

In this section we compare the mirror proton and neutron ANCs and analyze the Coulomb effects which are responsible for the difference between these ANCs. In what follows we simplify the notations for the proton and neutron ANCs omitting the quantum numbers and using just C_p and C_n , correspondingly. From Eq. (50) we get the ratio of the squares of the proton and neutron ANCs for mirror nuclei,

$$\begin{aligned} L_{pn}^W(R_{NA}) &= \frac{C_p^2}{C_n^2} = \left[\left(\frac{\kappa_{pA}^B}{\kappa_{nA}^{A+1}} \right)^{l_B} \frac{\Gamma(l_B + 1 + \eta_{pA}^{bs})}{\Gamma(l_B + 1)} \right. \\ &\quad \left. \times \frac{W_p(i\kappa_{pA}^B R_{NA})}{W_n(i\kappa_{nA}^{A+1} R_{NA})} \right]^2, \end{aligned} \quad (54)$$

where $W_p(i\kappa_{pA}^B R_{NA})$ ($W_n(i\kappa_{nA}^{A+1} R_{NA})$) is the Wronskian calculated for the proton (neutron) at the channel radius R_{NA} . To get the proton (neutron) Wronskian we can just replace in Eq. (51) $a \rightarrow p$ ($a \rightarrow n$). For the neutron Wronskian $\varphi_{l_B}(i\kappa_{nA}^{A+1} r_{nA}) = r_{nA}^{l_B+1} e^{-\kappa_{nA}^{A+1} r_{nA}} {}_1F_1(l_B + 1, 2l_B + 2; 2\kappa_{nA}^{A+1} r_{nA})$, where $\kappa_{nA}^{A+1} = \sqrt{2\mu_{nA} \varepsilon_{nA}^{A+1}}$ is the wave number of the bound state $A + 1 = (nA)$ of the isobaric analog state of the bound state $B = (pA)$.

Calculation of the ratio of the mirror nucleon ANCs requires knowledge of the microscopic radial overlap functions. In the meantime, in Ref. [28] another expression for the mirror nucleon ANCs ratio was obtained, which can be used when the overlap functions are not available. I show here how simple this derivation when using Eq. (54). First, as it was pointed out in Ref. [28], in the nuclear interior Coulomb interaction varies very little in the vicinity of R_{NA} and its effect leads only to shifting of the nucleon binding energy. Hence, we assume that $\varphi_{l_B}^C(i\kappa_{aA}^B r_{aA})$ and $\varphi_{l_B}(i\kappa_{aA}^B r_{aA})$ behave similarly at $r_{NA} \approx R_{NA}$ except for the overall normalization, that is,

$$\varphi_{l_B}^C(i\kappa_{pA}^B r_{pA}) = \frac{\varphi_{l_B}^C(i\kappa_{pA}^B R_{NA})}{\varphi_{l_B}(i\kappa_{nA}^{A+1} R_{NA})} \varphi_{l_B}(i\kappa_{nA}^{A+1} r_{pA}). \quad (55)$$

Then Eq. (54) reduces to

$$L_{pn}^{W'}(R_{NA}) = \frac{C_p^2}{C_n^2} \approx \left[\left(\frac{\kappa_{pA}^B}{\kappa_{nA}^{A+1}} \right)^{l_B} \frac{\Gamma(l_B + 1 + \eta_{pA}^{bs})}{\Gamma(l_B + 1)} \frac{\varphi_{l_B}^C(i\kappa_{pA}^B R_{NA})}{\varphi_{l_B}(i\kappa_{nA}^{A+1} R_{NA})} \frac{W[I_{pAl_B j_B J_B}^B(r_{pA}), \varphi_{l_B}(i\kappa_{nA}^{A+1} r_{pA})] \Big|_{r_{pA}=R_{NA}}}{W[I_{nAl_B j_B J_B}^{A+1}(r_{nA}), \varphi_{l_B}(i\kappa_{nA}^{A+1} r_{nA})] \Big|_{r_{nA}=R_{NA}}} \right]^2. \quad (56)$$

Neglecting further the difference between the proton and the neutron mirror overlap functions in the nuclear interior we obtain the approximate ratio of the squares of the mirror ANCs from [28] (in the notations of the current

paper):

$$L_{pn}(R_{NA}) = \frac{C_p^2}{C_n^2} \approx \left[\left(\frac{\kappa_{pA}^B}{\kappa_{nA}^{A+1}} \right)^{l_B} \frac{\Gamma(l_B + 1 + \eta_{pA}^{bs})}{\Gamma(l_B + 1)} \frac{\varphi_{l_B}^C(i \kappa_{pA}^B R_{NA})}{\varphi_{l_B}(i \kappa_{nA}^{A+1} R_{NA})} \right]^2. \quad (57)$$

In descending accuracy I can rank Eq. (54) as the most accurate, then Eq. (56) and then Eq. (57). Taking into account that the microscopic overlap functions (calculated in the no-core-shell-model [44–46], the variational Monte Carlo method [47–49], or the oscillator shell-model [41]) are more accurate in the nuclear interior, using Eq. (54) one can determine the ratio of the mirror ANCs quite accurately. Then follows Eq. (56), in which only one approximation (55) is used, and finally Eq. (57), in which two approximations are used. Equations (54) and (56) require knowledge of two mirror overlap nucleon functions, while to calculate Eq. (57) one does not need overlap functions and it is the simplest to estimate. As we see below, while ratio (54) practically does not depend on the channel radius R_{NA} , ratios (56) and (57) show some evident dependence on R_{NA} .

Now we explain physics causing the difference between the proton and neutron mirror ANCs. First of all the proton ANC is affected by the main CRF \mathcal{R}_1 [see Eq. (27)]. Eliminating this major factor from the proton ANC we obtain the ratio of the squares of the Coulomb renormalized proton and neutron ANCs:

$$\tilde{L}_{pn}^W(R_{NA}) = \frac{\tilde{C}_p^2}{C_n^2} = \left[\left(\frac{\kappa_{pA}^B}{\kappa_{nA}^{A+1}} \right)^{l_B} \frac{W_p(i \kappa_{pA}^B R_{NA})}{W_n(i \kappa_{nA}^{A+1} R_{NA})} \right]^2, \quad (58)$$

$$\tilde{L}_{pn}^{W'}(R_{NA}) = \frac{\tilde{C}_p^2}{C_n^2} \approx \left[\left(\frac{\kappa_{pA}^B}{\kappa_{nA}^{A+1}} \right)^{l_B} \frac{\varphi_{l_B}^C(i \kappa_{pA}^B R_{NA})}{\varphi_{l_B}(i \kappa_{nA}^{A+1} R_{NA})} \frac{W[I_{pA}^B l_B j_B J_B(r_{pA}), \varphi_{l_B}(i \kappa_{nA}^{A+1} r_{pA})] \Big|_{r_{pA}=R_{NA}}}{W[I_{nA}^{A+1} l_B j_B J_B(r_{nA}), \varphi_{l_B}(i \kappa_{nA}^{A+1} r_{nA})] \Big|_{r_{nA}=R_{NA}}} \right]^2, \quad (59)$$

and

$$\tilde{L}_{pn} = \frac{\tilde{C}_p^2}{C_n^2} \approx \left[\left(\frac{\kappa_{pA}^B}{\kappa_{nA}^{A+1}} \right)^{l_B} \frac{\varphi_{l_B}^C(i \kappa_{pA}^B R_{NA})}{\varphi_{l_B}(i \kappa_{nA}^{A+1} R_{NA})} \right]^2. \quad (60)$$

These ratios still may be far from unity. After we removed the main CRF, there are two more remaining CRFs, which determine the difference between the proton and neutron mirror ANCs. The second factor appears because of the difference in the proton and neutron binding energies. The dependence of the ANC on the binding energy is exponential [39]. Because the binding energy of the neutron analog state is larger than the corresponding proton binding energy, the renormalized squared proton ANC \tilde{C}_p^2 is lower than C_n^2 , and the second CRF decreases the proton ANC: the bigger the difference $\varepsilon_{nA}^{A+1} - \varepsilon_{pA}^B$ the stronger is the decrease of the proton ANC. The third CRF, which increases the proton ANC compared to the neutron one, is generated by the fine Coulomb effects (the effects left after removal the main CRF and difference in the binding energies) and is minor compared to the first two CRFs. Now after this discussion we can rewrite Eq. (58) as

$$\tilde{L}_{pn}^W(R_{NA}) = \tilde{\mathcal{R}}_2^W \tilde{\mathcal{R}}_3^W, \quad (61)$$

where

$$\tilde{\mathcal{R}}_2^W = \left[\left(\frac{\kappa_{pA}^B}{\kappa_{nA}^{A+1}} \right)^{l_B} \frac{W_n(i \kappa_{pA}^B R_{NA})}{W_n(i \kappa_{nA}^{A+1} R_{NA})} \right]^2 \quad (62)$$

and

$$\tilde{\mathcal{R}}_3^W = \left| \frac{W_p(i \kappa_{pA}^B R_{NA})}{W_n(i \kappa_{pA}^B R_{NA})} \right|^2. \quad (63)$$

To calculate the binding energy effect $\tilde{\mathcal{R}}_2^W$ on the ANCs ratio it is enough to replace in Eq. (58) the proton Wronskian $W_p(i \kappa_{pA}^B R_{NA})$ with the neutron one $W_n(i \kappa_{pA}^B R_{NA})$ but calculated at the proton binding energy. To calculate the impact of the fine Coulomb effects it is enough to consider the ratio of the squared proton and neutron Wronskians both calculated at the proton binding energy. Similarly we can estimate these renormalization effects for $\tilde{L}_{pn}^{W'}(R_{NA})$. For the ratio of the ANCs \tilde{L}_{pn} considered in Ref. [28] we get

$$\tilde{L}_{pn} = \tilde{\mathcal{R}}_2 \tilde{\mathcal{R}}_3, \quad (64)$$

where

$$\tilde{\mathcal{R}}_2 = \left[\left(\frac{\kappa_{pA}^B}{\kappa_{nA}^{A+1}} \right)^{l_B} \frac{\varphi_{l_B}(i \kappa_{pA}^B R_{NA})}{\varphi_{l_B}(i \kappa_{nA}^{A+1} R_{NA})} \right]^2 \quad (65)$$

is the CRF determining the effect of the binding energy, while

$$\tilde{\mathcal{R}}_3 = \left[\frac{\varphi_{l_B}^C(i \kappa_{pA}^B R_{NA})}{\varphi_{l_B}(i \kappa_{pA}^B R_{NA})} \right]^2 \quad (66)$$

is the CRF determining the fine Coulomb effects.

Thus, we can express the squared proton ANC in terms of the mirror squared neutron one as

$$C_p^2 = \mathcal{R}_1 \tilde{\mathcal{R}}_2^W \tilde{\mathcal{R}}_3^W C_n^2 \quad (67)$$

or

$$C_p^2 = \mathcal{R}_1 \tilde{\mathcal{R}}_2 \tilde{\mathcal{R}}_3 C_n^2, \quad (68)$$

depending on whether we use the Wronskian approach or more simple renormalization from [28]. Here we took into account that the quantum numbers of the proton and neutron analog states are the same.

Because I do not have all the required overlap functions, which are necessary to calculate the CRFs, only the renormalization factors $\tilde{\mathcal{R}}_2$ and $\tilde{\mathcal{R}}_3$ are estimated in Sec. V.

V. CALCULATIONS

In this section we consider some cases applying both Wronskian formalism and Eqs. (56) and (57).

Comparison of ANCs for $^{41}\text{Sc}(1f_{7/2}; 0.0 \text{ MeV}) \rightarrow ^{40}\text{Ca}(0.0 \text{ MeV}) + p$ and $^{41}\text{Ca}(1f_{7/2}; 0.0 \text{ MeV}) \rightarrow ^{40}\text{Ca}(0.0 \text{ MeV}) + n$. I start from analysis of the mirror proton and neutron ANCs for $^{41}\text{Sc}(1f_{7/2}; 0.0 \text{ MeV}) \rightarrow ^{40}\text{Ca}(0.0 \text{ MeV}) + p$ and $^{41}\text{Ca}(1f_{7/2}; 0.0 \text{ MeV}) \rightarrow ^{40}\text{Ca}(0.0 \text{ MeV}) + n$, correspondingly. Both ANCs correspond to isobaric analog states in the mirror nuclei and we can apply the formalism discussed in the previous section. The overlap functions are taken from [41].

In Fig. 1 is shown the ratio of the ANCs calculated using the Wronskian formalism and approximations (56) and (57). While the ratio obtained in the Wronskian formalism remains practically constant, both approximated ratios depend on the channel radius R_{NA} . Note that the results obtained using approximations (56) and (57) are valid only at $R_{NA} \leq R_A$, where $R_A \approx 4.5 \text{ fm}$ is the radius of $A = ^{40}\text{Ca}$. Equation (56) agrees better with the exact Wronskian expression than

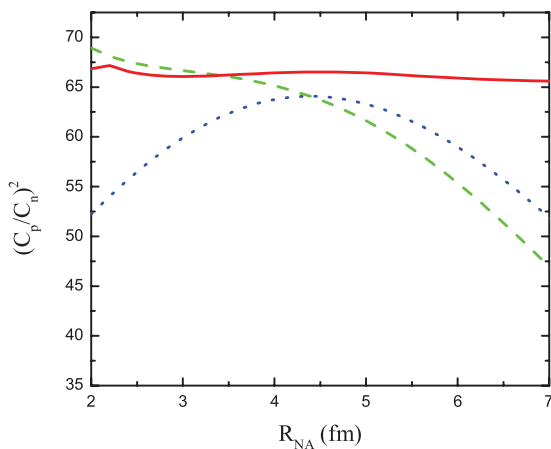


FIG. 1. (Color online) Ratio of the square of the proton ANC for the virtual decay $^{41}\text{Sc}(1f_{7/2}; 0.0 \text{ MeV}) \rightarrow ^{40}\text{Ca}(0.0 \text{ MeV}) + p$ to the square of the neutron ANC for the mirror nucleus virtual decay $^{41}\text{Ca}(1f_{7/2}; 0.0 \text{ MeV}) \rightarrow ^{40}\text{Ca}(0.0 \text{ MeV}) + n$. Solid red line, Wronskian method [Eq. (54)]; green dashed line, obtained using Eq. (56); dotted blue line, obtained using Eq. (57) as in Ref. [28].

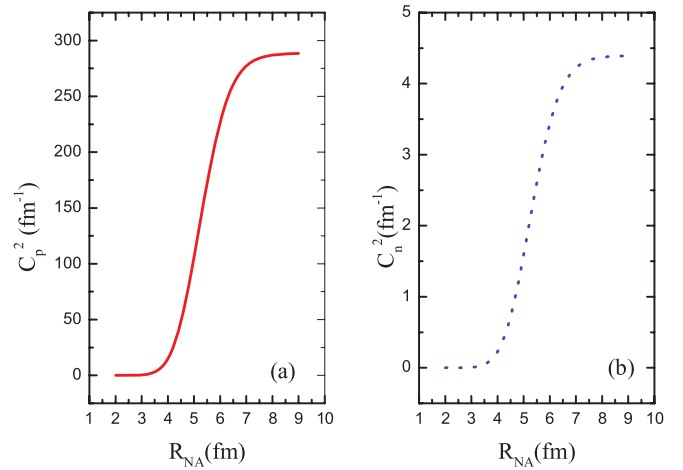


FIG. 2. (Color online) (a) Solid red line, dependence on R_{NA} of the square of the proton ANC for the virtual decay $^{41}\text{Sc}(1f_{7/2}; 0.0 \text{ MeV}) \rightarrow ^{40}\text{Ca}(0.0 \text{ MeV}) + p$ calculated using the Wronskian expression given by Eq. (50). (b) Blue dotted line, dependence on R_{NA} of the square of the neutron ANC for the virtual decay $^{41}\text{Ca}(1f_{7/2}; 0.0 \text{ MeV}) \rightarrow ^{40}\text{Ca}(0.0 \text{ MeV}) + n$ calculated using the Wronskian expression given by Eq. (50).

Eq. (57). The latter has the smallest deviation from the exact result at $R_{NA} \approx 4.4$.

In Fig. 2 the dependence on R_{NA} of the square of the proton and neutron ANCs for the virtual decays $^{41}\text{Sc}(1f_{7/2}; 0.0 \text{ MeV}) \rightarrow ^{40}\text{Ca}(0.0 \text{ MeV}) + p$ and $^{41}\text{Ca}(1f_{7/2}; 0.0 \text{ MeV}) \rightarrow ^{40}\text{Ca}(0.0 \text{ MeV}) + n$ calculated using the Wronskian expression given by Eq. (50). Comparison of Figs. 1 and 2 is very instructive. As we can conclude from the latter the ANCs calculated using the Wronskian method reach their correct values at $R_{NA} > 7 \text{ fm}$. In other words, only at $R_{NA} > 7 \text{ fm}$ the proton and neutron overlap functions can be replaced by their asymptotic terms. However, the ratio of the ANCs calculated using the Wronskian formalism remains constant practically at all $R_{NA} > 2$, allowing one to calculate this ratio even in the nuclear interior, where the overlap functions cannot be replaced by their asymptotic terms. Calculated using the Wronskian method, the proton and neutron ANCs and their ratios are in excellent agreement with the calculations in Ref. [41].

Now we consider how the Coulomb renormalization affects the proton ANC $C_p^2 = 286.9 \text{ fm}^{-1}$. There are three CRFs. Dividing the the proton squared ANC by each of these factors we can eliminate step by step all three Coulomb effects eventually arriving at the neutron squared ANC. To estimate the different CRFs I use Eqs. (65) and (66). The Wronskian formalism also could be used but not all the needed overlap functions are available. The main CRF in the case under consideration is $\mathcal{R}_1 = 14311.9$. Hence, the Coulomb renormalized square of the proton ANC is $\tilde{C}_p^2 = C_p^2 / \mathcal{R}_1 = 0.02 \text{ fm}^{-1}$. Now we take into account the remaining two CRFs coming from difference in the proton and neutron binding energies and the residual Coulomb effects. Because at $R_{NA} = 4.45 \text{ fm}$ the ratio of the proton and neutron ANCs obtained using Eq. (57) is the closest to the one obtained by the Wronskian method, the remaining two

Coulomb renormalizations are calculated at $R_{NA} = 4.45$ fm. The binding energy of the proton in $^{41}\text{Sc}(0.0 \text{ MeV})$ is $\varepsilon_p^{41\text{Sc}} = 1.085$ MeV, while the neutron binding energy in $^{41}\text{Ca}(0.0 \text{ MeV})$ is $\varepsilon_n^{41\text{Ca}} = 8.362$ MeV. This large difference in the neutron and proton binding energies leads to significant renormalization of the proton ANC compared to the neutron one. Dividing \tilde{C}_p^2 by the CRF $\mathcal{R}_2 = 0.0011$ we get the renormalized proton ANC at the neutron binding energy: $\tilde{C}_p'^2 = 18.18 \text{ fm}^{-1}$. Finally, dividing it by the CRF $\mathcal{R}_3 = 4.16$, reflecting the residual Coulomb effects, we get the square of the neutron ANC $C_n^2 = 4.37 \text{ fm}^{-1}$. These calculations clearly demonstrate the scale of the different CRFs leading to the difference between the mirror proton and neutron ANCs.

Let us consider now the ratio of the proton and neutron reduced widths for the mirror nuclei:

$$\frac{\gamma_p^2}{\gamma_n^2} = \frac{W_{-\gamma_p^b, l_B+1/2}^2(2\kappa_p R_{NA}) C_p^2}{W_{0, l_B+1/2}^2(2\kappa_n R_{NA}) C_n^2}. \quad (69)$$

For the case under consideration this ratio is $\gamma_p^2/\gamma_n^2 = 1.1$ at $R_{NA} = 4.45$ fm and gradually increasing with R_{NA} increase (see Fig. 3), demonstrating model dependence of the reduced widths. Because the ratio of the nucleon ANCs remains constant, the channel radius dependence comes entirely from the channel radius dependence of the Whittaker functions. The higher binding energy of the neutron generates stronger channel radius dependence of the neutron Whittaker function, which is actually proportional to the spherical Hankel function.

Comparison of ANCs for $^{17}\text{F}(1d_{5/2}; 0.0 \text{ MeV}) \rightarrow ^{16}\text{O}(0.0 \text{ MeV}) + p$ and $^{17}\text{O}(1d_{5/2}; 0.0 \text{ MeV}) \rightarrow ^{16}\text{O}(0.0 \text{ MeV}) + n$. As in the previous case, the overlap functions are nodeless at $r_{NA} > 0$ and I demonstrate how the Wronskian method works compared to approximated equations. I start from the analysis of the proton and neutron ANCs for $^{17}\text{F}(1d_{5/2}; 0.0 \text{ MeV}) \rightarrow ^{16}\text{O}(0.0 \text{ MeV}) + p$ and $^{17}\text{O}(1d_{5/2}; 0.0 \text{ MeV}) \rightarrow ^{16}\text{O}(0.0 \text{ MeV}) + n$, correspond-

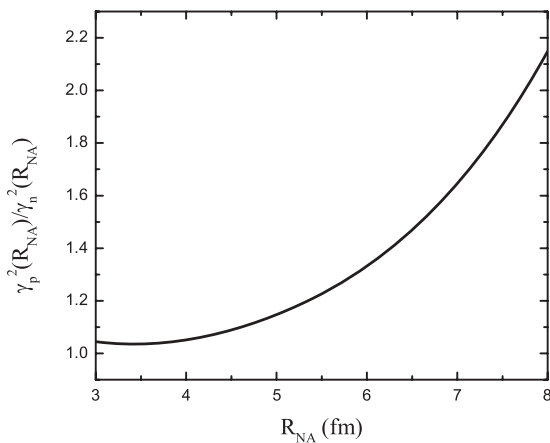


FIG. 3. The dependence on the channel radius of the ratio of the proton and neutron reduced widths for $^{41}\text{Sc}(1f_{7/2}; 0.0 \text{ MeV}) \rightarrow ^{40}\text{Ca}(0.0 \text{ MeV}) + p$ and $^{41}\text{Ca}(1f_{7/2}; 0.0 \text{ MeV}) \rightarrow ^{40}\text{Ca}(0.0 \text{ MeV}) + n$, correspondingly. The nucleon ANCs calculated using the Wronskian expression given by Eq. (50).

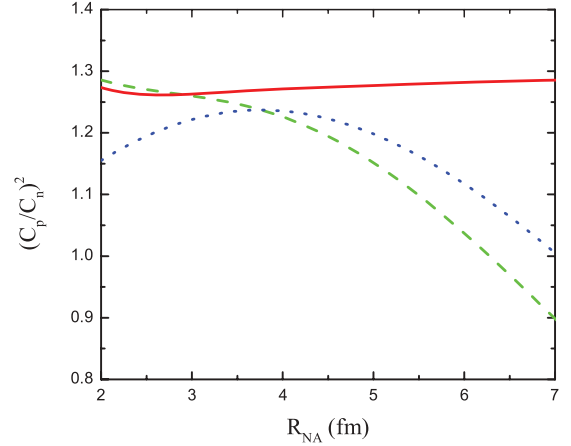


FIG. 4. (Color online) Ratio of the square of the proton ANC for the virtual decay $^{17}\text{F}(1d_{5/2}; 0.0 \text{ MeV}) \rightarrow ^{16}\text{O}(0.0 \text{ MeV}) + p$ to the square of the neutron ANC for the mirror nucleus virtual decay $^{17}\text{O}(1d_{5/2}; 0.0 \text{ MeV}) \rightarrow ^{16}\text{O}(0.0 \text{ MeV}) + n$. Solid red line, the Wronskian method [Eq. (54)]; green dashed line, obtained using Eq. (56); dotted blue line, obtained using Eq. (57) as in Ref. [28].

ingly. Both ANCs correspond to isobaric analog states in mirror nuclei and we can apply the formalism discussed in the previous section. The overlap functions are taken from [41].

In Fig. 4 the dependence on R_{NA} of the ratio of the mirror proton and neutron ANCs for the virtual decays $^{17}\text{F}(1d_{5/2}) \rightarrow ^{16}\text{O}(0.0 \text{ MeV}) + p$ and $^{17}\text{O}(1d_{5/2}) \rightarrow ^{16}\text{O}(0.0 \text{ MeV}) + n$ calculated using the Wronskian formalism and Eqs. (56) and (57) is shown. While the ratio obtained in the Wronskian formalism remains practically constant, Eqs. (56) and (57) provide the ratios which depend on the channel radius R_{NA} . Equation (56) agrees very well with the exact Wronskian method at $R_{NA} \leq 3$ fm. The assumption that the mirror proton and neutron overlap functions are close to each other in the nuclear interior is the basis for both approximate equations for the ANCs ratio. It is clear from Fig. 5 that with the R_{NA}

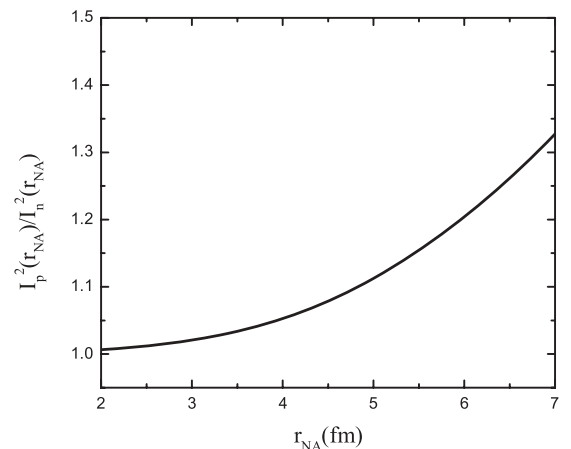


FIG. 5. Ratio of the square of the proton and neutron radial overlap functions for $^{17}\text{F}(1d_{5/2}; 0.0 \text{ MeV}) \rightarrow ^{16}\text{O}(0.0 \text{ MeV}) + p$ and $^{17}\text{O}(1d_{5/2}; 0.0 \text{ MeV}) \rightarrow ^{16}\text{O}(0.0 \text{ MeV}) + n$. The overlap functions are from [41].

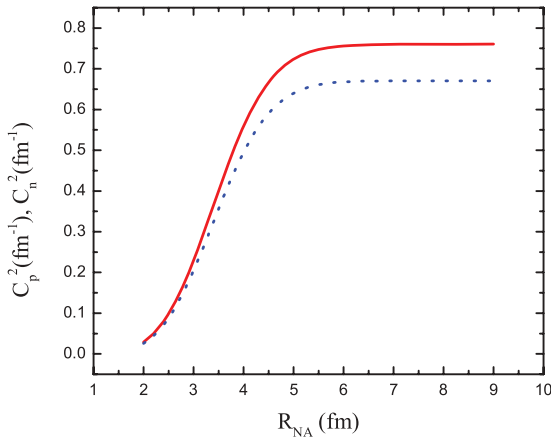


FIG. 6. (Color online) Dependence on R_{NA} of the square of the proton (solid red line) and neutron (blue dotted line) ANCs for the virtual decays $^{17}\text{F}(1d_{5/2}) \rightarrow ^{16}\text{O}(0.0 \text{ MeV}) + p$ and $^{17}\text{O}(1d_{5/2}) \rightarrow ^{16}\text{O}(0.0 \text{ MeV}) + n$, correspondingly, calculated using the Wronskian expression given by Eq. (50).

increase the square of the ratio of the mirror overlap functions deviates from unity.

A comparison of Figs. 4 and 6 is very instructive and shows the power of the Wronskian method. As is clear from Fig. 6, the proton and neutron ANCs calculated using the Wronskian equation reach their plateau only at $R_{NA} > 6$ fm. However, the ratio of the ANCs calculated using the Wronskian formalism [Eq. (54)] remains constant practically at all $R_{NA} > 2$ fm, allowing one to calculate this ratio even in the region where the overlap functions cannot be replaced by their asymptotic terms. The ratio of the proton and neutron ANCs calculated using approximated Eq. (56) agrees very well with the Wronskian method at $R_{NA} \leq 3$ fm, which is well in the nuclear interior, while Eq. (57) gives the ratio below the Wronskian method.

Now we consider how the Coulomb renormalization affects the proton ANC $C_p^2 = 0.58 \text{ fm}^{-1}$. To estimate the different CRFs I use, as in the previous case, Eqs. (65) and (66). The main CRF in the case under consideration is $\mathcal{R}_1 = 42.01$. Hence, the Coulomb renormalized square of the proton ANC is $\tilde{C}_p^2 = C_p^2/\mathcal{R}_1 = 0.0138 \text{ fm}^{-1}$. Now we take into account the remaining two CRFs coming from difference in the proton and neutron binding energies and the residual Coulomb effects. Because at $R_{NA} = 4.0$ fm the ratio of the proton and neutron ANCs obtained using Eq. (57) is the closest to the one obtained by the Wronskian method, the remaining two CRFs are calculated at $R_{NA} = 4.0$ fm. The binding energy of the proton in $^{17}\text{F}(0.0 \text{ MeV})$ is $\varepsilon_{p^{16}\text{O}}^{17\text{F}} = 0.605 \text{ MeV}$, while the neutron binding energy in $^{17}\text{O}(0.0 \text{ MeV})$ is $\varepsilon_{n^{16}\text{O}}^{17\text{O}} = 4.14 \text{ MeV}$. This large difference in the neutron and proton binding energies leads to significant renormalization of the proton ANC compared to the neutron one. Dividing \tilde{C}_p^2 by the CRF $\mathcal{R}_2 = 0.015$ we get the renormalized proton ANC at the neutron binding energy: $\tilde{C}_p'^2 = 0.92 \text{ fm}^{-1}$. Finally, dividing it by the CRF $\mathcal{R}_3 = 1.97$, reflecting the residual Coulomb effects, we get the square of the neutron ANC $C_n^2 = 0.467 \text{ fm}^{-1}$. These calculations once again demonstrate

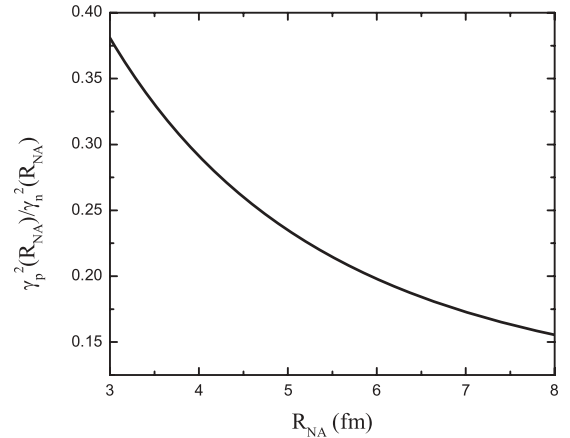


FIG. 7. Dependence on the channel radius of the ratio of the proton and neutron reduced widths for $^{17}\text{F}(1d_{5/2}; 0.0 \text{ MeV}) \rightarrow ^{16}\text{O}(0.0 \text{ MeV}) + p$ and $^{17}\text{O}(1d_{5/2}; 0.0 \text{ MeV}) \rightarrow ^{16}\text{O}(0.0 \text{ MeV}) + n$, correspondingly. The nucleon ANCs calculated using the Wronskian expression given by Eq. (50).

the scale of the different CRFs leading to the difference between the mirror proton and neutron ANCs.

The ratio of the proton and neutron reduced widths $\gamma_p^2/\gamma_n^2 = 0.29$ at $R_{NA} = 4.0$ fm and gradually decreasing with R_{NA} increase (see Fig. 7), demonstrating model dependence of the reduced widths. In this case the proton Whittaker function drops faster than the neutron one.

Comparison of ANCs for $^{17}\text{F}(2s_{1/2}) \rightarrow ^{16}\text{O}(0.0 \text{ MeV}) + p$ and $^{17}\text{O}(2s_{1/2}) \rightarrow ^{16}\text{O}(0.0 \text{ MeV}) + n$. In this section I analyze the ratio of the proton and neutron ANCs for $^{17}\text{F}(2s_{1/2}) \rightarrow ^{16}\text{O}(0.0 \text{ MeV}) + p$ and $^{17}\text{O}(2s_{1/2}) \rightarrow ^{16}\text{O}(0.0 \text{ MeV}) + n$, correspondingly. Both ANCs correspond to isobaric analog states in the mirror nuclei and we can apply the formalism discussed in the previous section. The overlap functions are taken from [41]. It is a special case because of the very low proton binding energy, $\varepsilon_{p^{16}\text{O}}^{17\text{F}} = 0.105 \text{ MeV}$. Besides, the overlap functions have one node at $r_{NA} > 0$ and it will be interesting to see how the Wronskian method works in this case. The ratio of the square of the proton and neutron overlap functions $I_p^2(r_{NA})/I_n^2(r_{NA}) > 1$ at all r_{NA} (see Fig. 8). Hence, both approximations (56) and (57) fail.

It is seen from Fig. 9 where the ratios of the ANCs calculated using the Wronskian formalism and Eqs. (56) and (57) are shown. While the ratio obtained in the Wronskian formalism remains practically constant at $R_{NA} > 4$ fm, the ratios obtained using Eqs. (56) and (57) depend on the channel radius R_{NA} and at the best radius $R_{NA} = 5$ fm underestimate the exact ratio (Wronskian equation) by 30%. The anomalous behavior of the Wronskian expression at $R_{NA} < 4$ fm is the result of the nodes of the overlap functions.

In Fig. 10 the dependence on R_{NA} of the square of the mirror proton and neutron ANCs for the virtual decays $^{17}\text{F}(2s_{1/2}) \rightarrow ^{16}\text{O}(0.0 \text{ MeV}) + p$ and $^{17}\text{O}(2s_{1/2}) \rightarrow ^{16}\text{O}(0.0 \text{ MeV}) + n$ calculated using the Wronskian expression given by Eq. (50). Owing to the low nucleon binding energies the nucleon overlap functions reach their asymptotic tail (the ANCs reach their plateau) only at $R_{NA} > 7$ fm (see Fig. 10). However, the

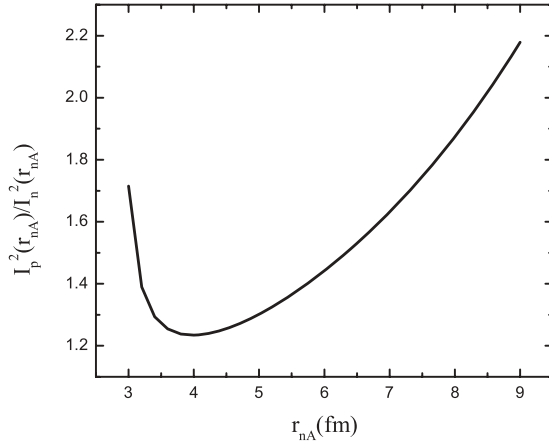


FIG. 8. Ratio of the square of the proton and neutron radial overlap functions for $^{17}\text{F}(2s_{1/2}) \rightarrow ^{16}\text{O}(0.0 \text{ MeV}) + p$ and $^{17}\text{O}(2s_{1/2}) \rightarrow ^{16}\text{O}(0.0 \text{ MeV}) + n$.

ratio of the ANCs calculated using the Wronskian formalism (see Fig. 9) remains practically constant at all $R_{nA} > 5$ fm, allowing one to calculate this ratio even in the region where the overlap functions cannot be replaced by their asymptotic terms. Note that, according to the calculations using the Wronskian method, the proton and neutron ANC and their ratios are in excellent agreement with the calculations in Ref. [41].

The ratio of the proton and neutron reduced widths $\gamma_p^2/\gamma_n^2 = 1.71$ at $R_{nA} = 5.0$ fm and gradually increasing with R_{nA} increase (see Fig 11), demonstrating model dependence of the reduced widths. In this case the neutron Whittaker function drops slightly faster than the proton one.

Comparison of ANCs for $^8\text{B}(1p_{3/2}; 0.0 \text{ MeV}) \rightarrow ^7\text{Be}(0.0 \text{ MeV}) + p$ and $^8\text{Li}(1p_{3/2}; 0.0 \text{ MeV}) \rightarrow ^7\text{Li}(0.0 \text{ MeV}) + n$. To analyze the mirror proton and neutron ANC for $^8\text{B}(1p_{3/2}; 0.0 \text{ MeV}) \rightarrow ^7\text{Be}(0.0 \text{ MeV}) + p$ and $^8\text{Li}(1p_{3/2}; 0.0 \text{ MeV}) \rightarrow ^7\text{Li}(0.0 \text{ MeV}) + n$ I use the overlap

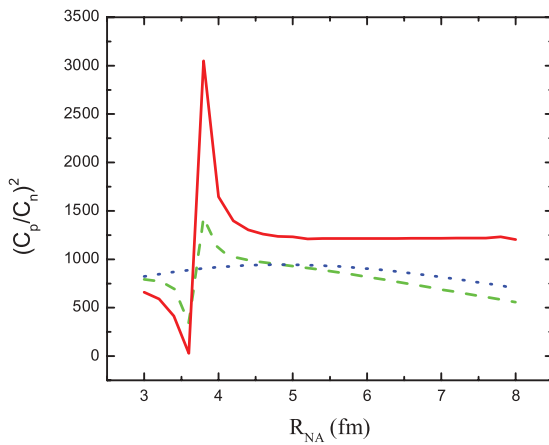


FIG. 9. (Color online) Ratio of the square of the proton ANC for the virtual decay $^{17}\text{F}(2s_{1/2}) \rightarrow ^{16}\text{O}(0.0 \text{ MeV}) + p$ to the square of the neutron ANC for the mirror nucleus virtual decay $^{17}\text{O}(2s_{1/2}) \rightarrow ^{16}\text{O}(0.0 \text{ MeV}) + n$. Solid red line, the Wronskian method [Eq. (54)]; green dashed line, obtained using Eq. (56); dotted blue line, obtained using Eq. (57) as in Ref. [28].

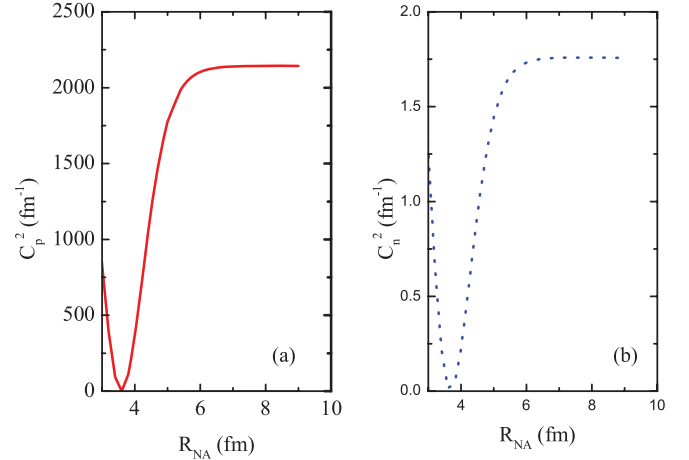


FIG. 10. (Color online) (a) Red solid line, dependence on R_{nA} of the square of the proton ANC for the virtual decay $^{17}\text{F}(2s_{1/2}) \rightarrow ^{16}\text{O}(0.0 \text{ MeV}) + p$ calculated using the Wronskian expression given by Eq. (50). (b) Blue dotted line, dependence on R_{nA} of the square of the neutron ANC for the virtual decay $^{17}\text{O}(2s_{1/2}) \rightarrow ^{16}\text{O}(0.0 \text{ MeV}) + n$ calculated using the Wronskian expression given by Eq. (50).

functions obtained from the variational Monte Carlo wave functions using the Green's function method [54].

In Fig. 12 the ratios of the square of the proton and neutron ANC calculated using the Wronskian formalism and Eqs. (56) and (57) are shown. The ratio obtained in the Wronskian formalism remains almost constant (the observed oscillations are related with the accuracy of the Monte Carlo method). The ratios obtained using Eqs. (56) and (57) in the internal region at $R_{nA} < 3.5$ fm are practically constant and lower than the exact ratio. The mean value of the calculated ratio of the square of the proton and neutron ANC using the Wronskian method in the interval 3.4–4.6 fm is 1.24, which is slightly higher than the experimental ratio 1.06 ± 0.11 [55] and the ratio 1.15 obtained using Eq. (57).

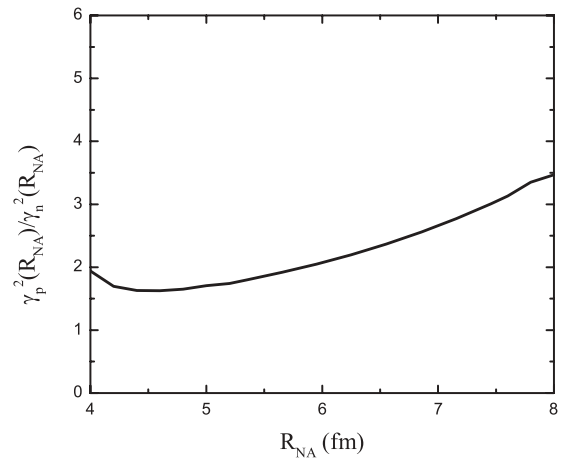


FIG. 11. The dependence on the channel radius of the ratio of the proton and neutron reduced widths for $^{17}\text{F}(2s_{1/2}; 0.0 \text{ MeV}) \rightarrow ^{16}\text{O}(0.0 \text{ MeV}) + p$ and $^{17}\text{O}(2s_{1/2}; 0.0 \text{ MeV}) \rightarrow ^{16}\text{O}(0.0 \text{ MeV}) + n$, correspondingly. The nucleon ANC calculated using the Wronskian expression given by Eq. (50).

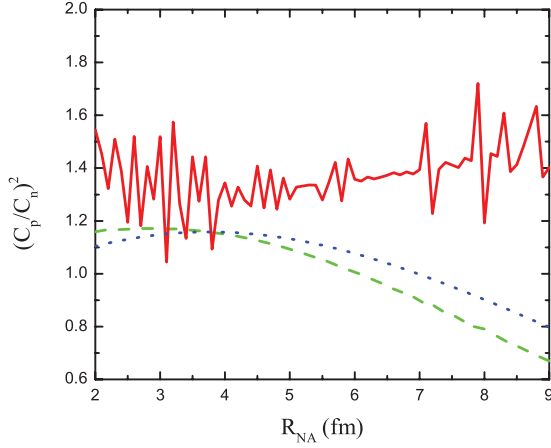


FIG. 12. (Color online) Ratio of the square of the proton ANC for the virtual decay ${}^8\text{B}(1p_{3/2}; 0.0 \text{ MeV}) \rightarrow {}^7\text{Be}(0.0 \text{ MeV}) + p$ to the square of the neutron ANC for the mirror nucleus virtual decay ${}^8\text{Li}(1p_{3/2}; 0.0 \text{ MeV}) \rightarrow {}^7\text{Li}(0.0 \text{ MeV}) + n$. Solid red line, the Wronskian method [Eq. (54)]; green dashed line, obtained using Eq. (56); dotted blue line, obtained using Eq. (57).

In Fig. 13 is shown the dependence on R_{NA} of the square of the proton and neutron ANCs for the virtual decays ${}^8\text{B}(1p_{3/2}; 0.0 \text{ MeV}) \rightarrow {}^7\text{Be}(0.0 \text{ MeV}) + p$ and ${}^8\text{Li}(1p_{3/2}; 0.0 \text{ MeV}) \rightarrow {}^7\text{Li}(0.0 \text{ MeV}) + n$, correspondingly, calculated using the Wronskian expression given by Eq. (50). As we can see, in contrast to the previous cases, the calculations using the Wronskian approach never reach plateau, which reflects the fact that the Monte Carlo overlap functions do not have correct asymptotic radial shape. Nevertheless, the ratio of the mirror proton and neutron ANCs, as is shown in Fig. 12, remains practically stable confirming once more that this ratio can be calculated with the overlap functions, which are correct only in the nuclear interior.

Once again we can estimate all the Coulomb renormalization effects on the proton ANC. We adopt the square

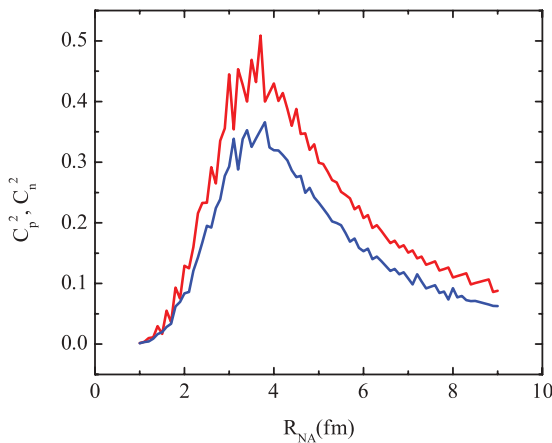


FIG. 13. (Color online) Red (blue) solid line, dependence on R_{NA} of the square of the proton (neutron) ANC for the virtual decay ${}^8\text{B}(1p_{3/2}; 0.0 \text{ MeV}) \rightarrow {}^7\text{Be}(0.0 \text{ MeV}) + p$ (${}^8\text{Li}(1p_{3/2}; 0.0 \text{ MeV}) \rightarrow {}^7\text{Li}(0.0 \text{ MeV}) + n$) calculated using the Wronskian expression given by Eq. (50).

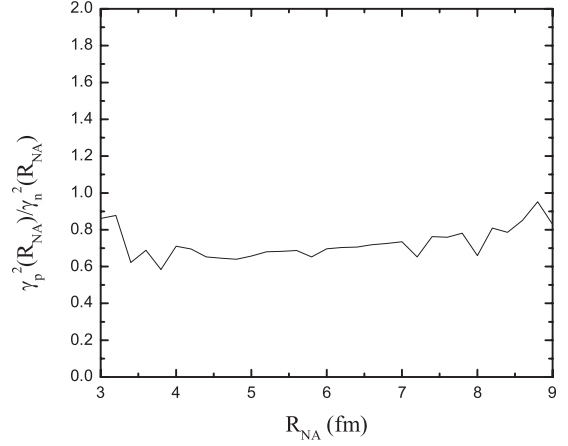


FIG. 14. Dependence on the channel radius of the ratio of the proton and neutron reduced widths for ${}^8\text{B}(1p_{3/2}; 0.0 \text{ MeV}) \rightarrow {}^7\text{Be}(0.0 \text{ MeV}) + p$ and ${}^8\text{Li}(1p_{3/2}; 0.0 \text{ MeV}) \rightarrow {}^7\text{Li}(0.0 \text{ MeV}) + n$, correspondingly. The nucleon ANCs calculated using the Wronskian expression given by Eq. (50).

of the ANC $C_p^2 = 0.43 \text{ fm}^{-1}$ obtained from the Wronskian expression at $R_{NA} = 4 \text{ fm}$. The main CRF in the case under consideration is $\mathcal{R}_1 = 13.66$. The Coulomb renormalized square of the proton ANC is $\tilde{C}_p^2 = 0.0315 \text{ fm}^{-1}$. Now we take into account the remaining two Coulomb renormalizations coming from difference in the proton and neutron binding energies and the residual Coulomb effects. The binding energy of the proton in ${}^8\text{B}(0.0 \text{ MeV})$ is $\varepsilon_p^{{}^8\text{B}} = 0.1375 \text{ MeV}$, while the neutron binding energy in ${}^8\text{Li}(0.0 \text{ MeV})$ is $\varepsilon_n^{{}^8\text{Li}} = 2.03 \text{ MeV}$. The difference between the proton and neutron binding energies leads to renormalization of the proton ANC compared to the neutron one. Dividing \tilde{C}_p^2 by the CRF at $R_{NA} = 4 \text{ fm}$ $\mathcal{R}_2 = 0.053$ we get the renormalized proton ANC at the neutron binding energy: $\tilde{C}_p'^2 = 0.59 \text{ fm}^{-1}$. Finally, dividing it by the CRF at $R_{NA} = 4 \text{ fm}$ $\mathcal{R}_3 = 1.61$, reflecting the residual Coulomb effects, we get the square of the neutron ANC $C_n^2 = 0.37 \text{ fm}^{-1}$.

The ratio of the proton and neutron reduced widths for ${}^8\text{B}(1p_{3/2}; 0.0 \text{ MeV}) \rightarrow {}^7\text{Be}(0.0 \text{ MeV}) + p$ and ${}^8\text{Li}(1p_{3/2}; 0.0 \text{ MeV}) \rightarrow {}^7\text{Li}(0.0 \text{ MeV}) + n$, correspondingly (see Fig. 14), gradually increases with R_{NA} increase.

VI. SUMMARY

The first goal of this paper is to analyze the Coulomb renormalization of the ANC. It is shown that the Coulomb renormalization of the proton ANC compared to the neutron one of the mirror nucleus consists of three factors. First is the main CRF given by Eq. (27). The second CRF is the result of the decrease of the proton binding energy compared to the neutron one and the third CRF is the result of the fine Coulomb effects (residual Coulomb effects after removing the main CRF). The scale of each CRF is determined for different cases. I also draw attention to the possibility of using the renormalized ANC when the standard one becomes too large.

The second important result of this paper is the derivation of a new expression for the ratio of the proton and neutron ANC's for isobaric analog states of the mirror nuclei. This equation is obtained from the Pinkston-Satchler equation and given by the ratio of the Wronskians taken from the radial overlap functions and regular solutions of the two-body $N + A$ radial Schrödinger equation with the short-range interaction excluded. It is shown that, by using microscopic overlap functions, which are more accurate in the nuclear interior, one can determine the ratio of the mirror nucleon ANC's which are the amplitudes of the tails of the corresponding overlap functions. It allows us to obtain one of the nucleon ANC's if other is known. The results of this paper can be extended for

the resonance states (when the overlap functions for resonance states will be available) and for the arbitrary mirror ANC's for the systems $a + A$, for example, for $a = \alpha$.

ACKNOWLEDGMENTS

The work was supported by the US Department of Energy under Grants No. DE-FG02-93ER40773, No. DE-FG52-09NA29467, and No. DE-SC0004958 (topical collaboration TORUS) and NSF under Grant No. PHY-0852653. The author expresses his thanks to N. K. Timofeyuk, K. M. Nollett, and R. B. Wiringa for presenting the overlap functions.

-
- [1] L. D. Blokhintsev, I. Borbely, and E. I. Dolinskii, *Fiz. Elem. Chastits At. Yadra* **8**, 1189 (1977) [*Sov. J. Part. Nuclei* **8**, 485 (1977)].
- [2] L. D. Blokhintsev, A. M. Mukhamedzhanov, and A. N. Safronov, *Fiz. Elem. Chastits At. Yadra* **15**, 1296 (1984) [*Sov. J. Part. Nuclei* **15**, 580 (1984)].
- [3] A. M. Mukhamedzhanov and R. E. Tribble, *Phys. Rev. C* **59**, 3418 (1999).
- [4] E. I. Dolinsky and A. M. Mukhamedzhanov, *Izv. N. SSSR, Ser. Fiz.* **41**, 2055 (1977) [*Bull. Acad. Sci. USSR, Phys. Ser.* **41**, 55 (1977)].
- [5] A. M. Mukhamedzhanov and N. K. Timofeyuk, *Pis'ma Eksp. Teor. Fiz.* **51**, 247 (1990) [*JETP Lett.* **51**, 282 (1990)].
- [6] A. M. Mukhamedzhanov and N. K. Timofeyuk, *Sov. J. Nucl. Phys.* **51**, 431 (1990) [*Yad. Fiz.* **51**, 679 (1990)].
- [7] A. M. Mukhamedzhanov, C. A. Gagliardi, and R. E. Tribble, *Phys. Rev. C* **63**, 024612 (2001)..
- [8] A. M. Mukhamedzhanov, L. D. Blokhintsev, and B. F. Irgaziev, *Phys. Rev. C* **83**, 055805 (2011).
- [9] Xiaodong Tang, A. Azhari, C. A. Gagliardi, A. M. Mukhamedzhanov, F. Pirlpepov, L. Trache, R. E. Tribble, V. Burjan, V. Kroha, and F. Carstoiu, *Phys. Rev. C* **67**, 015804 (2003).
- [10] A. M. Mukhamedzhanov, M. La Cognata, and V. Kroha, *Phys. Rev. C* **83**, 044604 (2011).
- [11] H. A. Kramers, *Hand Jahrb. Chem. Phys.* **1**, 312 (1938).
- [12] M. Perelomov, V. S. Popov, M. V. Terentev, *Zh. Eksp. Teor. Fiz.* **51**, 309 (1966).
- [13] W. Heisenberg, *Z. Naturforsch.* **1**, 608 (1946).
- [14] C. Möller, *Dan. Vid Selsk. Mat. Fys. Medd.* **22**, 19 (1946).
- [15] N. Hu, *Phys. Rev.* **74**, 131 (1948).
- [16] As a matter of fact, in these works the ANC was the amplitude of the bound-state wave function of two structureless particles.
- [17] Ya. B. Zel'dovich, *Zh. Eksp. Teor. Fiz.* **51**, 1492 (1965).
- [18] H. M. Xu, C. A. Gagliardi, R. E. Tribble, A. M. Mukhamedzhanov, and N. K. Timofeyuk, *Phys. Rev. Lett.* **73**, 2027 (1994).
- [19] A. M. Mukhamedzhanov, R. P. Schmitt, R. E. Tribble, and A. Sattarov, *Phys. Rev. C* **52**, 3483 (1995).
- [20] A. M. Mukhamedzhanov *et al.*, *Phys. Rev. C* **67**, 065804 (2003).
- [21] A. M. Mukhamedzhanov *et al.*, *Phys. Rev. C* **73**, 035806 (2006).
- [22] A. Banu *et al.*, *Phys. Rev. C* **79**, 025805 (2009).
- [23] T. Al-Abdullah *et al.*, *Phys. Rev. C* **81**, 035802 (2010).
- [24] A. M. Mukhamedzhanov *et al.*, *Phys. Rev. C* **78**, 015804 (2008).
- [25] E. G. Adelberger *et al.*, *Rev. Mod. Phys.* **83**, 195 (2011).
- [26] A. M. Mukhamedzhanov and A. S. Kadyrov, *Phys. Rev. C* **82**, 051601(R) (2010).
- [27] A. M. Mukhamedzhanov, *Phys. Rev. C* **84**, 044616 (2011).
- [28] N. K. Timofeyuk, R. C. Johnson, and A. M. Mukhamedzhanov, *Phys. Rev. Lett.* **91**, 232501 (2003).
- [29] N. K. Timofeyuk and P. Descouvemont, *Phys. Rev. C* **72**, 064324 (2005).
- [30] N. K. Timofeyuk, D. Baye, P. Descouvemont, R. Kamouni, and I. J. Thompson, *Phys. Rev. Lett.* **96**, 162501 (2006).
- [31] J. Okolowicz, N. Michel, W. Nazarewicz, and M. Ploszajczak, *Phys. Rev. C* **85**, 064320 (2012).
- [32] L. J. Titus, P. Capel, and F. M. Nunes, *Phys. Rev. C* **84**, 035805 (2011).
- [33] E. D. Johnson *et al.*, *Phys. Rev. Lett.* **97**, 192701 (2006).
- [34] W. T. Pinkston and G. R. Satchler, *Nucl. Phys.* **72**, 641 (1965)
- [35] R. J. Philpott, W. T. Pinkston, and G. R. Satchler, *Nucl. Phys. A* **119**, 241 (1968).
- [36] D. Y. Wong and H. P. Noyes, *Phys. Rev.* **126**, 1866 (1962).
- [37] Yu. L. Mentkovsky, *Nucl. Phys.* **65**, 673 (1965).
- [38] J. Hamilton *et al.*, *Nucl. Phys.* **60**, 443 (1973).
- [39] A. I. Baz', Ya. B. Zel'dovich, and A. M. Perelomov, *Scattering, Reactions and Decay in Nonrelativistic Quantum Mechanics*, 2nd ed. (Nauka, Moscow, 1971) [English translation of 1st ed. (Jerusalem, 1969)].
- [40] L. D. Blokhintsev and A. N. Safronov, *Izv. Acad. Nauk SSSR* **47**, 2168 (1983).
- [41] N. K. Timofeyuk, *Phys. Rev. C* **84**, 054313 (2011).
- [42] N. K. Timofeyuk, *Nucl. Phys. A* **632**, 19 (1998).
- [43] R. G. Newton, *Scattering Theory of Waves and Particles*, 2nd ed. (Springer-Verlag, Heidelberg, 1982).
- [44] P. Navratil, J. P. Vary, and B. R. Barrett, *Phys. Rev. C* **62**, 054311 (2000).
- [45] P. Navratil and W. E. Ormand, *Phys. Rev. C* **68**, 034305 (2003).
- [46] S. Quaglioni and P. Navratil, *Phys. Rev. Lett.* **101**, 092501 (2008).
- [47] C. S. Pieper and R. B. Wiringa, *Ann. Rev. Nucl. Part. Sci.* **51**, 53 (2001).
- [48] K. M. Nollett, S. C. Pieper, R. B. Wiringa, J. Carlson, and G. M. Hale, *Phys. Rev. Lett.* **99**, 022502 (2007).
- [49] Kenneth M. Nollett and R. B. Wiringa, *Phys. Rev. C* **83**, 041001 (2011).

- [50] O. Jensen, G. Hagen, M. Hjorth-Jensen, B. A. Brown, and A. Gade, *Phys. Rev. Lett.* **107**, 032501 (2011).
- [51] A. S. Kadyrov, I. Bray, A. M. Mukhamedzhanov, and A. T. Stelbovics, *Ann. Phys.* **324**, 1516 (2009).
- [52] A. M. Mukhamedzhanov, *Phys. Rev. C* **84**, 044616 (2011).
- [53] A. M. Mukhamedzhanov and A. S. Kadyrov, *Phys. Rev. C* **82**, 051601(R) (2010).
- [54] K. M. Nollett, arXiv:1206.0046 (2012).
- [55] L. Trache, A. Azhari, F. Carstoiu, H. L. Clark, C. A. Gagliardi, Y.-W. Lui, A. M. Mukhamedzhanov, X. Tang, N. Timofeyuk, and R. E. Tribble, *Phys. Rev. C* **67**, 062801(R) (2003).